Inceptor counteracts insulin signalling in β-cells to control glycaemia

by

Ansarullah[1,12,14], Chirag Jain[1,12,14], Fataneh Fathi Far[1,9,14], Sarah Homberg[1,9,14], Katharina Wißmiller[1,9,14], Felizitas Gräfin von Hahn[1,9,14], Aurelia Raducanu[1,12], Silvia Schirge[1,12], Michael Sterr[1,9,12], Sara Bilekova[1,9], Johanna Siehler[1,9], Julius Wiener[2,10], Lena Oppenländer[1,9], Amir Morshedi[1], Aimée Bastidas-Ponce[1,9,12], Gustav Collden[7], Martin Irmler[3,12], Johannes Beckers[3,8,12], Annette Feuchtinger[4], Michal Grzybek[11,12], Christin Ahlbrecht[6,12,13], Regina Feederle[5], Oliver Plettenburg[6,12,13], Timo D. Müller[7,12], Matthias Meier[2,10], Matthias H. Tschöp[7,9,12], Ünal Coskun[10,12] and Heiko Lickert[1,9,12]

[1]Institute of Diabetes and Regeneration Research, [2]Helmholtz Pioneer Campus, Helmholtz Center Munich, Neuherberg, Germany, [3]Institute of Experimental Genetics, [4]Core Facility Pathology and Tissue Analytics, [5]Monoclonal Antibody Core Facility, [6]Institute for Medicinal Chemistry, [7]Institute of Diabetes and Obesity at the Helmholtz Center Munich, 85764 Neuherberg Germany; [8]Chair of Experimental Genetics, School of Life Sciences Weihenstephan, Technische Universität München, Freising, Germany, [9]Technical University of Munich, School of Medicine, 81675 Munich, Germany, [10]IMTEK, Department of Microsystems Engineering, University of Freiburg, 79110 Freiburg, Germany, [11]Paul Langerhans Institute Dresden of Helmholtz Center Munich, Technical University Dresden, 01062 Dresden, Germany; [12]German Center for Diabetes Research (DZD), 85764 Neuherberg, Germany; [13]Institute of Organic Chemistry, Center of Biomolecular Research, Leibniz Universität Hannover, 30167 Hannover.

[14]These authors contributed equally to this work.

Correspondence and requests for materials should be addressed to H.L. (heiko.lickert@helmholtz-muenchen.de)

Heiko Lickert, Helmholtz Center Munich, Ingolstaedter Landstraße 1, 85764, Neuherberg, Germany. PHONE: +49 89 31873760, FAX: +49 89 31873761.

Summary

Insulin and insulin-like growth factor 1 (Igf1) resistance in pancreatic β-cells causes overt diabetes, thus, therapeutic improvement may protect from β-cell failure[1-3]. Here, we identified a novel inhibitor of insulin (Insr) and Igf1 receptor (Igf1r) signalling in β-cells, which we named insulin inhibitory receptor (Inceptor; *Iir*). Inceptor contains an extracellular cysteine-rich domain with similarities to the Insr and Igf1r[4] and a mannose-6-phosphate domain found in the Igf2r[5]. Inceptor knock-out (KO) mice die within the first hours after birth with signs of hyperinsulinemia and hypoglycaemia. Molecular and cellular analysis of the *Iir*$^{-/-}$ embryonic and postnatal pancreas showed increased Insr/Igf1r activation, resulting in augmented β-cell proliferation and mass. Similarly, inducible β-cell-specific *Iir*$^{-/-}$ KO in adult mice and in *ex vivo* islets led to increased Insr/Igf1r activation and β-cell proliferation, resulting in improved glucose tolerance *in vivo*. Mechanistically, Inceptor interacts with Insr and Igf1r to facilitate clathrin-mediated endocytosis for receptor desensitisation. Blocking this physical interaction using monoclonal antibodies against the extracellular domain of Inceptor retained Inceptor and Insr at the plasma membrane to sustain Insr/Igf1r activation in β-cells. Taken together, Inceptor shields insulin-producing β-cells from constitutive pathway activation and provides a molecular target for Insr/Igf1r sensitisation and potential diabetes therapy. (197 words)

The overall β-cell mass is determined by a balance between β-cell neogenesis, proliferation and apoptosis. There is plenty of evidence that insulin/Igf1 signalling regulates β-cell function, homeostasis and proliferation[3]. Specifically, knock-out of Insr in β-cells impairs compensatory β-cell proliferation upon genetic or diet-induced insulin resistance[6] and causes loss of β-cell mass and increased apoptosis[1,2,7,8]. Furthermore, high-fat diet-induced hyperinsulinemia drives the expansion of β-cells mass dependent on dynamic changes in insulin levels[9]. Lastly, total insulin and Igf1 resistance in pancreatic β-cells causes overt diabetes in mice[1,2] and likely contributes to the pathophysiology in humans[3]. Thus, insulin sensitisation may protect and/or regenerate β-cells for diabetes remission.

Upon ligand binding, Insr and Igf1r homo- and heterodimers quickly get auto-phosphorylated via their receptor tyrosine kinase (RTK) domains and activate shared downstream kinases, including Raf-1/MEK/ERK1-2, PI3K/AKT and mTOR[10,11], which in turn regulate growth, survival, proliferation and metabolism. Desensitisation of RTK signalling is facilitated by either clathrin- or caveolin-mediated endocytosis[12-14]. It has been questioned if autocrine insulin action in β-cells makes physiological sense[15], as prolonged exposure to insulin leads to insulin resistance[16]. Unfortunately, insulin concentration in pancreatic islets cannot be measured *in vivo*, but mathematical modelling predicts dynamic concentrations that activate the Insr and likely also the Igf1r[17]. This supports the idea that auto- and paracrine signalling regulates β-cell function, proliferation and survival[3]. Surprisingly, although β-cells are the source of insulin, it is currently not known if pancreatic islets and β-cells are shielded from constitutive pathway activation. Based on these findings, we hypothesize that mechanisms must have evolved to desensitise Insr/Igf1r signalling in the pancreas and β-cells to counteract insulin resistance and uncontrolled growth and proliferation.

Results

Discovery of insulin inhibitor receptor

In screens to identify novel pancreatic regulators, we recently identified the *5330417C22Rik* mRNA to be strongly expressed in the pancreas at embryonic stage (E)14.5 (Extended Data Fig. 1a). The human gene is known as estrogen-induced gene (*EIG121*) or *KIAA1324* and has been mainly described in the context of cancer[18,19]. The murine gene is located on chromosome 3 and has 22 exons being transcribed via three alternative splice-variants and translated into a single-pass type I transmembrane protein (Extended Data Fig. 2a-c). Bioinformatic analyses revealed conservation of cysteine-residues in the growth factor receptor cysteine-rich domain (CRD)[4] when compared with the CRD of Insr and Igf1r (Fig. 1a; Extended Data Fig. 2c and 3a, b). In addition, the mannose-6-phosphate receptor binding domain shows similarities to the cation-dependent (CD-M6PR) and the cation-independent mannose-6-phosphate receptor (CI-M6PR/Igf2r) (Extended Data Fig. 3c, d)[5]. Due to similarities to Insr, Igf1r and Igf2r in the extracellular domain and its inhibitory function (see below), we renamed the protein insulin inhibitory receptor (Inceptor; *Iir*). Unlike Insr and Igf1r, Inceptor lacks a receptor tyrosine kinase domain, but contains a short cytoplasmic tail with a consensus binding motif for the AP2 adaptor complex which is involved in clathrin-mediated endocytosis (CME) (Extended Data Fig. 2d).

To get a better idea of Inceptor protein and *Iir* mRNA and expression, we performed further bioinformatic analyses. According to the EMBL-EBI expression atlas the *Iir* mRNA was mainly detected in secretory cells of endocrine glands and the hypothalamic-pituitary-gonadal axis (data not shown). To study the Inceptor expression and function in detail, we affinity purified the human INCEPTOR ectodomain (Extended Data Fig. 4a) and used a peptide with a conserved C-terminal

sequence to generate several specific mono- and polyclonal antibodies detecting the extracellular and cytoplasmic domain of mouse and human INCEPTOR (Extended Data Fig. 4b-g). Immunohistochemically we localized Inceptor within endocrine and exocrine cells in the embryonic (E14.5-18.5) and adult pancreas and islets (Fig. 1b-c; Extended Data Fig. 1e). Taken together, the high expression of Inceptor in the embryonic pancreas when peak numbers of insulin-producing β-cells are born and its similarities in secondary domain structure to Insr, Igf1r and Igf2r, suggested a functional role in regulating insulin/IGF signalling in the pancreas.

Inceptor regulates β-cell mass and glycemia

To test this hypothesis, we generated a full-body KO (*Iir*$^{-/-}$) and confirmed that no Inceptor protein was synthesized in the pancreas (Extended Data Fig. 4e, 5a, b). *Iir*$^{-/-}$ animals were born at the expected Mendelian ratio without any developmental defects or alterations in body weight, but died within 5 h postpartum (Fig. 1d, Extended Data Fig. 1b). Gross morphological analysis showed no obvious differences between *Iir*$^{+/+}$ and *Iir*$^{-/-}$ pancreata (Fig. 1e). Interestingly, *Iir*$^{-/-}$ neonates showed significantly lower fasting blood glucose levels compared to *Iir*$^{+/+}$ at 2-5 h postpartum, which correlated with the observed increased serum insulin levels and higher hepatic glycogen content (Fig. 1f-h). 50% of the newborn pups could be rescued with glucose injections (Extended Data Fig. 1g). In addition, the *Iir*$^{-/-}$ pups exhibited increased glucose tolerance (Extended Data Fig. 1h). Endocrine proliferation was significantly increased during pancreas development at E16.5 (Fig. 1i, Extended Data Fig. 1f), whereas ductal, endocrine and exocrine differentiation was not affected at E14.5-18.5 (Extended Data Fig. 1e). Accordingly, determination of the β-cell area at E19.5 revealed a slight, but significant increase in insulin-secreting cells accompanied by a higher total pancreatic insulin content in *Iir*$^{-/-}$ neonates (Fig. 1j, k). No alterations in

serum glucagon levels or α-cell area were observed (Extended Data Fig. 1c, d). Thus, *Iir* KO leads to increased β-cell proliferation and mass during pancreas development leading to alteration of glucose homeostasis after birth.

To better understand the postnatal lethality and molecular function of Inceptor in the pancreas, we analysed global mRNA expression profiles of *Iir*$^{+/+}$ and *Iir*$^{-/-}$ pancreata before and after birth. Principal component analysis revealed strong gene expression changes when neonates switched from maternal to autonomous metabolic control (Fig. 1l; PC1: 30.7% variance). *Iir*$^{+/+}$ vs *Iir*$^{-/-}$ pancreata did not differ in gene expression before birth at E18.5, but after birth at P0 (Fig. 1i; PC2: 9.3% variance). Gene ontology terms analysis revealed that genes activated during starvation (autophagy and mitophagy) or ER stress were upregulated, whereas genes regulating metabolism, mitochondrial oxidative phosphorylation and pancreatic exocrine secretion were downregulated (Fig. 1m), which was further confirmed by quantitative PCR analysis (Extended Data Fig.1i). Notably, genes involved in the IGFR, PI3K-Akt and FoxO signalling were differentially regulated and signalling analysis revealed Insr/Igf1r overactivation in *Iir*$^{-/-}$ pancreata at E18.5 (Fig. 1m-o).

To circumvent postnatal lethality and to study the function of Inceptor specifically in adult β-cells and glucose homeostasis, we generated a tamoxifen-inducible conditional β-cell specific KO (MIP-CreERT; *Iir*$^{flox/FD}$), hereafter named CKO (Extended Data Fig. 5a-d). Four weeks post-tamoxifen injection, specific deletion of *Iir* in β-cells was confirmed and no obvious change in islet composition was observed at 4 months of age (Fig. 2a, Extended Data Fig. 5h). Body weight, fasting glucose and serum insulin levels did not differ between control and CKO mice (Fig. 2b-c; Extended Data Fig. 5e). However, CKO mice showed an improved glucose tolerance along with increased first

phase insulin secretion after glucose injection (Fig. 2d-f). The β-cell proliferation rate and mass were increased in CKO mice, while the α-cell mass and β-cell maturation markers (UCN3, MafA) remained unchanged (Fig. 2g-i, Extended Data Fig. 5f, i). Similar to embryonic pancreata at E18.5, we observed overactivation of Insr/Igf1r before and after insulin stimulation and increased Akt activation after insulin stimulation in CKO islets *ex vivo* (Fig. 2j, k). Furthermore, tamoxifen-induced *Iir* deletion in isolated islets *in vitro* also revealed increased Insr/Igf1r phosphorylation after insulin stimulation which resulted in an increased β-cell proliferation (EdU) (Fig. 2l-n, Extended Data Fig. 5g).

Inceptor facilitates clathrin-mediated endocytosis

To understand how Inceptor antagonizes Insr/Igf1r signalling on the cellular and molecular level, we first analysed the subcellular localization of the protein in the murine Min6 β-cell insulinoma line. Proteins with M6PR domains, such as the CI-M6PR/Igf2r[5], function in trafficking of lysosomal enzymes from the trans-Golgi network to endosomes and their subsequent transport to lysosomes. Consistently, Inceptor is localized on the subcellular level mainly in the endoplasmic reticulum (ER)-Golgi intermediate compartment (Ergic53), trans-Golgi (Tgn46) and cis-medial (Gianti, Gm130) Golgi network and is partially localized in endosomes (Rab7, EEA1) and lysosomes (Lamp1 and Lamp2) as shown by co-localization studies (Fig. 3a, b, Extended Data Fig. 6a). Furthermore, we identified several motifs in the cytoplasmic domain for the interaction with the coatomer complex COPI (KxxK, KxKxx or KxE) that is involved in retrograde transport from the trans- to the cis-Golgi network and ER and we detected co-expression of Inceptor and CM1 (Extended Data Fig. 2d, 6a). A small fraction of Inceptor was located at the plasma membrane as detected by an antibody specific to the extracellular domain in non-permeabilized cells (Fig. 3c). In endocytosis

assays, we observed that Inceptor antibodies were quickly internalized from the plasma membrane and routed to the Golgi-ER-lysosome compartment (Fig. 3d-f; Extended Data Fig. 6b-e). Furthermore, Inceptor co-localized with clathrin found in clathrin-coated pits (CCP) (Fig. 3b), exhibited proximity to AP2 (Fig. 3g, h) and harbours a YxxxΘ AP2 binding motif (YSKL) (Extended Data Fig. 2d), suggesting that Inceptor is internalized via CME. To directly test this idea, we introduced a site-specific mutation and changed the consensus AP2 binding motif YSKL to ASKA (INCEPTOR-AP2*-Venus) and compared the subcellular localization to INCEPTOR-Venus. INCEPTOR-Venus was localized comparable to endogenous Inceptor, whereas INCEPTOR-AP2*-Venus was found to a lesser extent in the Golgi area and negatively correlated with clathrin staining (Extended Data Fig. 6f, g). Notably, mutation of the AP2 binding motif in the cytoplasmic domain of INCEPTOR and/or treatment of Dynasore (a CME inhibitor) in INCEPTOR-Venus expressing cells resulted in retention at the plasma membrane (Fig. 3i-j; Extended Data Fig. 8a, b). Taken together, Inceptor shares intracellular trafficking routes with the Igf2r scavenger receptor[5] and is internalized from the plasma membrane by CME, i.e. in the same way as the activated Insr complex and other RTKs[12-14].

Inceptor desensitises insulin signalling in β-cells

To explore whether Inceptor is involved in Insr and/or Igf1r internalization and desensitisation, we tested physical interactions by co-immunoprecipitations and proximity-ligation experiments. Interestingly, we could detect Inceptor both in the eluate of immunoprecipitated endogenous Insr and Igf1r from Min6 cells and mouse WT islets, while stimulation with insulin further increased the physical interaction (Fig. 4a-b; Extended Data Fig. 7a, b). This suggested that Inceptor directly or indirectly interacts either with Insr or Igf1r homodimers or with Insr/Igf1r heterodimers. The

physical interaction was confirmed on a single-cell subcellular level which further revealed that Inceptor co-localizes in 50 nm close proximity to activated Insr/Igf1r complexes (Fig. 4c, d; Extended Data Fig. 7c). The internalization of monovalent labelled insulin-AlexaFluor546 was reduced in *Iir*$^{-/-}$ when compared to *Iir*$^{+/+}$ Min6 as well as in primary islet cells, suggesting a role of Inceptor in Insr/Igf1r desensitisation after CME (Fig. 4e, Extended Data Fig. 7d-f). Recently it was shown that the activated Insr can be internalized via the recruitment of the AP2 complex and specifically the AP2M1 subunit to a juxtamembrane domain[13,14]. To test if Inceptor directly or indirectly interacts with the Insr/Igf1r complex we co-immunoprecipitated Inceptor with pAP2M1, the active form of AP2M1 subunit at the plasma membrane. We could detect an endogenous interaction of Inceptor and pAP2M1 in Min6 cells and show that the protein-protein interaction of pAP2M1 with INCEPTOR-Venus depends on the AP2 binding motif (YSKL) (Extended Data Fig. 8c-e). Furthermore, overexpression of INCEPTOR-Venus stabilizes the active pAP2M1 and total levels of AP2M1 and decreased p-Insr/Igf1r levels, suggesting that Inceptor directly recruits AP2M1 to facilitate CME for desensitization of Insr (Extended Data Fig. 8f-i). Interestingly, a monoclonal antibody (mAb) directed against the extracellular domain of INCEPTOR, but not its isotype control, could sensitise Insr/Igf1r and its downstream signalling in Min6 and EndoC-βH1 cells (Fig. 4f-g; Extended Data Fig. 9a, b). Analysis of the surface receptors by surface biotinylation, precipitation and quantification revealed that Inceptor, but not isotype control mAb led to plasma membrane retention of Inceptor and Insr, both in mouse Min6 as well as in human EndoC-βH1 cells (Fig. 4h-i, Extended Data Fig. 7g, 9c, d). This in turn led to increased Insr/Igf1r activation, likely by interfering with the kinetics of the steady-state of endocytosis and recycling of Inceptor and Insr. In consequence, Inceptor desensitises Insr/Igf1r signalling by CME in β-cells where it could be a target to increase functional β-cell mass.

Understanding the molecular mechanisms regulating Insr/Igf1r signalling and feedback regulation is important for β-cell protection and regeneration[1-3]. Here we have identified the insulin inhibitory receptor (Inceptor) as a novel negative regulator of the Ins/Igf1 signalling pathway that effectively desensitises Insr and Igf1r after pathway activation in β-cells. This offers a mechanistic explanation of how β-cells exist at highest concentrations of insulin and target receptors (Insr and Igf1r), but are still shielded from insulin resistance. Thus, INCEPTOR is a novel molecular target to sensitise INSR/IGF1R signalling in human β-cells to prevent β-cell failure and overt diabetes.

Figure legends:

Fig. 1 | Inceptor is highly expressed in the pancreas, regulates endocrine cell proliferation and Ins/Igf1 signalling.

a, Scheme of Inceptor predicted domain structure

b-c, Inceptor expression in endocrine (white arrow) and exocrine cells (yellow arrow) in the embryonic pancreas (b) and adult islets (c). Scale bar 50 μm

d, Mendelian ratio and representative image of a P0litter

e, Images showing gross morphology of pancreata at E19.5. Scale bar 2 mm

f-h, Fasting blood glucose levels (f; n=19, $Iir^{+/+}$; n=15, $Iir^{-/-}$; P<0.0001), serum insulin levels (g; n=44, $Iir^{+/+}$; n=45, $Iir^{-/-}$; P<0.0001) and hepatic glycogen content (h; n=15, $Iir^{+/+}$; n=8, $Iir^{-/-}$; P<0. 0194) of pups at E19.5. Data are mean ± s.e.m. Significance was calculated using unpaired t-test

i, Endocrine cell proliferation in *Iir*$^{+/+}$ and *Iir*$^{-/-}$ pancreata at E16.5-18.5 (*n*=3; data are mean ± s.e.m.; *P*=0.03 at E16.5). Each n represents 3-8 quantified LSM-images (see Extended Data Fig. 1). Significance was calculated using unpaired t-test

j, β-cell area of *Iir*$^{+/+}$ and *Iir*$^{-/-}$ pancreata at E19.5 mice (*n*=5; data are mean ± s.e.m.; *P*=0.0438). Significance was calculated using unpaired t-test**k**, Total pancreatic insulin content of *Iir*$^{+/+}$ and *Iir*$^{-/-}$ mice at P0 (*n*=8; data are mean ± s.e.m.*P*<0.05). Significance was calculated using unpaired t-test

l, Principal component analysis of the gene expression profiles from pancreata of 5 h starved pups before (*n*=5, *Iir*$^{+/+}$; *n*=4 *Iir*$^{-/-}$) and after birth (*n*=5, *Iir*$^{+/+}$; *n*=6, *Iir*$^{-/-}$)

m, Functional enrichment analysis was performed on of differentially expressed genes (P0 KO vs WT, p<0.01, fold change >1.5) using Homer (v.4.10)

n-o, Western blot analysis (**n**) and quantification (**o**) of insulin signalling in pancreata of 4 h starved pups at E18.5. (Data are mean ± s.e.m ; *n*=3 mice; p-Insr/Igf1r, *P*=0.002; Insr, *P*=0.0002; Igf1r, *P*=0.1464). Significance was calculated using unpaired t-test

Fig. 2 | Tamoxifen-inducible β-cell specific knock-out of Inceptor causes increased Insr/Igf1r signalling and β-cell proliferation leading to improved glucose tolerance

a, Immunofluorescent analysis showing β-cell specific deletion efficiency of Inceptor from CKO (MIP-CreERT+; *Iir*$^{fl/FD}$, tamoxifen) and control (MIP-CreERT+; *Iir*$^{fl/+}$,

tamoxifen). (**a-k**) 16 month male mice 4 weeks post tamoxifen administration. Scale bar 50 μm

b-c, Fasting blood glucose levels (b; n=30, control; n=14, CKO) and fasting serum insulin levels (c; n=10, control; n=8, CKO). Data are mean ± s.e.m. No significant changes were observed.

d-e, Blood glucose levels during an intraperitoneal glucose tolerance test in control (n=12) and CKO (n=15) (**d**). Data are mean ± s.e.m; *$P \leq 0.05$,**$P \leq 0.01$,***$P \leq 0.001$. Significance was calculated by two-way ANOVA followed by Bonferroni's multiple comparisons test. Area under curve (AUC) of ipGTT (**e**). Significance was calculated by unpaired t-test. Data are mean ± s.e.m;**$P \leq 0.01$

f, Serum insulin levels during an *in vivo* intraperitoneal glucose stimulated insulin secretion in control (n=7) and CKO (n=8). Data are mean ± s.e.m;* $P \leq 0.05$. Significance was determined using two-way ANOVA followed by Bonferroni's multiple comparisons test

g, β-cell mass of CKO (n=3) and control (n=4) mice. Data are mean ± s.e.m; $P=0.07$. Significance calculated by unpaired t-test

h-i, Images from control (n=3) and CKO (n=3) mice immunostained with insulin (magenta), glucagon (green) and EdU (white) (**h**). Scale bar, 50 μm. Quantification of β-cell proliferation (%) of $EdU^{+}Ins^{+}$ co-positive cells (white arrows) in control and CKO mice (**i**). Data are mean ± s.e.m, $P=0.08$. Significance was calculated by unpaired t-test

j-k Western blot analysis (**j**) and quantification (**k**) of islets isolated from control (n=3) and CKO (n=3) mice stimulated in the absence or presence of 100 nM insulin for 5

min. Data are mean ± s.e.m;*$P \leq 0.05$,** $P \leq 0.01$,*** $P \leq 0.001$. Significance was calculated by two-way ANOVA followed by Bonferroni's multiple comparisons test.

l-m, Western blot analysis (l) and quantification (m) of *in vitro* induced deletion of Inceptor in control (n=3) and CKO (n=3) islets stimulated with 100 nM insulin for 15 min. Data are mean ± s.e.m;*$P \leq 0.05$,**$P \leq 0.01$,*** $P \leq 0.001$. Significance was calculated by unpaired t-test

n, Quantification of β-cell proliferation (EdU) of *in vitro* tamoxifen induced deletion of Inceptor in islets.. Data are mean ± s.e.m; n=4; * $P \leq 0.05$. Significance was calculated by unpaired t-test

Fig. 3 │ Inceptor is mainly localized in the Golgi-ER-lysosomal compartment and internalized via clathrin-mediated endocytosis

a, Scheme of clathrin-mediated endocytosis of Inceptor and its routing in the ER-Golgi and endosomal-lysosomal compartments.

b, Confocal images showing the co-localization of Inceptor (green) with TGN46, Rab7, Lamp2 or clathrin (magenta) and quantified by Pearson correlation coefficient (*n* = 3; TGN46, 210; Rab7, 303; Lamp2, 267; clathrin 248 cells in total). Scale bar 5 µm.

c, Confocal image showing the localization of Inceptor (green) at the plasma membrane marked by ConA (magenta) and total Inceptor (cyan). Scale bar 20 µm.

d, Experimental design forendocytosis assay.

e-f, Confocal images (**e**) and quantification (**f**) with a Pearson correlation coefficience of GM130 (magenta) and Inceptor (green) at 30 and 60 min (Data are mean ± s.e.m; n = 1421 cells in total). Scale bar 5 µm.

g-h, Images (**g**) and quantification (**h**) for the proximity ligation of Inceptor and AP2 in *Iir*$^{+/+}$ and *Iir*$^{-/-}$ Min6 cells. Potential interactions were quantified as fluorescent dots/cell. (P=2.12e^{-12}, n = 8147 cells). *** P≤0.001. Significance was calculated using an unpaired, two-samples Wilcoxon test. Scale bar 50 µm.

i-j, Immunostaining (i) and quantification (j) showing localization of INCEPTOR-Venus or INCEPTOR-AP2*-Venus (green) at the plasma membrane (CellMask, red). (Data are mean ± s.e.m; ~40 *Iir*$^{+/+}$ and *Iir*$^{-/-}$ cells/n. * P≤0.05, P=0.02, n=3). Significance was calculated using an unpaired t-test. Scale bar 10 µm.

Fig. 4 | Inceptor physically interacts with Insr and Igf1r to enhance receptor internalization and desensitisation

a-b, Co-immunoprecipitation of endogenous Inceptor with Insr and Igf1r in Min6 cells using anti-Insr antibody (top panel, n=4) or Igf1r antibody (middle panel, n=5) under different metabolic conditions (**a**) Box and whisker plots (min to max) showing relative density (fold change) of proteins (**b**). Data are mean ± s.e.m; each 'n' represents biologically independent samples; *P≤0.05,**P≤0.01,***P≤0.001. Significance was calculated using one-way ANOVA followed by Bonferroni's multiple comparisons test.

c-d, Proximity ligation assay for endogenous Inceptor alone or together with Insr, Igf1r and p-Igf1r in Min6 cells (c) and quantified fluorescent dots/cell (d). (Inceptor,

P=1.4e^{-9}, n = 5544 cells; Inceptor+Insr, P=0.0051, n = 3837 cells; Inceptor+Igf1r, P=0.0051, n=3067 cells; Inceptor+p-Igf1r, P=0.0051, n=2798 cells). Data are mean ± s.e.m, **P≤0.01,***P≤0.001. Significance was calculated using an unpaired, two-sample Wilcoxon test. Scale bar, 50 μm. See Extended Data Fig. 7a for negative control.

e, Quantification of the uptake of insulin-546 by Insr/Igf1r at different time points in Min6 *Iir*$^{+/+}$ and *Iir*$^{-/-}$ cells (P=0.023; 150 cells/experiment and each time point, n=5). Data are mean ± s.e.m, *P≤0.01. Significance was calculated using two-way ANOVA followed by Bonferroni's multiple comparisons test.

f-g, Western blot analysis (h) and quantification (i) from Min6 cells under growth conditions treated with rat anti-INCEPTOR mAb and IgG2b (control) for 5 min at three different concentrations. n=3 biologically independent samples; data are mean ± s.e.m. *P≤0.05, **P≤0.01,***P≤0.001. Significance was calculated using a two-way ANOVA followed by Bonferroni's multiple comparisons test.

h-i, Surface biotinylation assay showing surface pools of Inceptor, p-Insr/Igf1r, Insr and Igf1r in Min6 cells treated with IgG2b control and anti-INCEPTOR mAb (1μg/mL) (h) and quantification (i). (n = 4 biologically independent samples; data are mean ± s.e.m. *P≤0.05,**P≤0.01,*** P≤0.001. Significance was calculated using a two-way ANOVA followed by Sidak's multiple comparisons test. See Extended Data Fig. 7g for input controls.

Methods

Data reporting

No statistical methods were used to predetermine sample size. The experiments were not randomized and the investigators were not blinded.

Animal studies, generation of full and conditional knock-out mice

Animal experiments were carried out in compliance with the German Animal Protection Act and with the approved guidelines of the Society of Laboratory Animals (GV-SOLAS) and of the Federation of Laboratory Animal Science Associations (FELASA). Mouse lines used (for targeting strategy see Extended Data Fig. 4a): Full knock-out, *Iir*$^{-/-}$*; 5330417C22Rik*$^{tm1a(EUCOMM)Hmgu}$ embryonic stem cells were aggregated with CD1 morula to generate chimeric mice. GeneTrap mice were bred on a mixed background. For critical exon deletion, GeneTrap animals were crossed with *Rosa26R-Cre* to generate *Iir*$^{+/-}$ animals used for intercrosses to obtain *Iir*$^{-/-}$. Conditional *knock-out* (CKO), *MIP-CreERT*^{1} *Iir*$^{fl/FD}$: GeneTrap animals were crossed with *FlpE* to obtain *Iir*$^{+/fl}$ followed by further crossing with *Rosa26R-Cre* to generate *Iir*$^{+/FD}$ animals. *MIP-CreERT*$^{+}$*, Iir*$^{+/FD}$ were mated with *Iir*$^{fl/fl}$ to obtain *MIP-CreERT*$^{+}$*, Iir*$^{fl/FD}$ (CKO) animals. Conditional deletion from 12 weeks old mice was achieved by intraperitoneal injections of tamoxifen (Sigma-Aldrich #T5648) three times every 48 h at a dose of 100 mg/kg body weight. For genotyping, primer sequences for *Iir* were: 5'-*CACCTCCCCCTGAACCTGAAAC*-3'; 5'-*GATGCCTGTCAGCCTTCATC*-3'; 5'-*GAGTGGGATGAGCTACCTCAC*-3'. Band sizes: *Iir*$^{+/+}$ = 341 bp; *Iir*$^{-/-}$ = 266 bp. Primer sequences for *MIP-CreERT*$^{+}$: 5'-*CCTGGCGATCCCTGAACATGTCCT*-3'; 5'-*TGGACTATAAAGCTGGTGGGCAT*-3'. Bandsize: *CreERT*$^{+}$ = 280bp. Primer sequences for *Iir*$^{fl/FD}$: 5'-*GGAACTTCGTCGAGATAACTTCGTATAG*-3'; 5'-

363 *GTGCACTCTGGGTAGTGTTC*-3'; 5'-*CCAAGGCCAGCGATACAACC*-3'. Band size:
364 $Iir^{+/+}$ = 395 bp; $Iir^{fl/fl}$ = 431 bp, $Iir^{FD/FD}$ = 285 bp.
365

366 ***Metabolic parameters***

367 Pregnant dams were starved for 2 h prior to C-section at E19.5. Fasting blood glucose
368 levels in the pups were measured using a glucometer (FreeStyle™/Bayer Contour
369 next) or using enzymatic kits as per the manufacturer's protocol (Wako #298-65701).
370 Quantification of circulating serum insulin, C-peptide and glucagon were assayed in
371 serum using commercial mouse-specific ELISA kits (CrystalChem, #90080, #90050,
372 Mercodia #10-1281-01). For rescue experiments, $Iir^{-/-}$ newborns and their littermates
373 were administered D-glucose (10%, 50 µl per injection; *s.c*) just after birth and every
374 6 h thereafter up to 24 h. For assessing glucose tolerance, $Iir^{-/-}$ newborns and their
375 littermates were administered a single injection of D-glucose (10%, 50 µl per injection;
376 *s.c*). Briefly, an individual P0 pup would receive glucose and then be sacrificed at a
377 predefined time point (0, 30, 60, 90 or 120 min). For each time point 4-12 pups were
378 used for analysis. For pancreatic insulin content, whole pancreases at P0 stage were
379 homogenized and incubated overnight in acid-ethanol buffer at 4°C and subsequently
380 quantified using mouse-specific ELISA kit. Liver glycogen levels were quantified using
381 a colorimetric assay kit according to the manufacturer's protocol (Abcam, #ab65620).
382

383 ***Immunohistochemistry***

384 Pancreata were fixed overnight at 4°C in 4% PFA, dehydrated in a sucrose gradient
385 (7.5-30%) and embedded in tissue freezing medium (Leica) before cutting sections of
386 10-20 µm thickness. After permeabilization in 0.25–0.5% Triton-X 100, slides were
387 treated with or without glycine (100 mM) for 30 min at RT and followed by blocking for
388 another 1 h. Primary antibodies were incubated overnight at 4°C using the following

antisera guinea pig anti-insulin (Thermo Scientific, #PA1-26938,1:50-1:1000), rabbit anti-E-Cadherin (CST, #3195, 1:500); rabbit anti-Foxa2 (CST, #8186, 1:300); goat anti-chromogranin A (SCBT, #sc-1488, 1:100 -200); rabbit anti-insulin (CST, #3014, 1:300); guinea pig anti-glucagon (Takara Bio, #M182, 1:2500); goat anti-somatostatin (SCBT, #sc-7819, 1:300); goat anti-pancreatic polypeptide (Abcam, #ab15580, 1:300); rabbit anti-α amylase (Abcam, #ab21156, 1:400); rabbit anti-Sox9 (Millipore, #AB5535, 1:300); rabbit anti-Urocortin3 (Phoenix Pharmaceuticals, #H-019-29, 1:300); rabbit anti-MafA (Novusbio, #NBP1-00121, 1:300). Slides were then washed 3 times and incubated with fluorophore-conjugated secondary antibodies for 2 h at RT in the dark using the following antibodies at 1:800 dilutions: donkey anti-rabbit Alexa Fluor® 555 (1:800, Invitrogen, #A31572); donkey anti-guinea pig Alexa Fluor® 649 (Dianova, #706-495-148); donkey anti-mouse Alexa Fluor® 488 (Invitrogen, #A21202); donkey anti-rabbit Alexa Fluor® 488 (Invitrogen, #A21206); donkey anti-goat Alexa Fluor® 594 (Invitrogen, #A11058); donkey anti-guinea pig Alexa Fluor® 488 (Dianova, #706-545-148); donkey anti-rat Alexa Fluor® 488 (Invitrogen, #A21208); donkey anti-goat Alexa Fluor® 555 (Invitrogen, #A21432); donkey anti-rabbit Alexa Fluor® 594 (Invitrogen, A21207); donkey anti-rat Alexa Fluor® 649 (Dianova, #712-605-150); donkey anti-goat Alexa Fluor® 488 (Invitrogen, #A11055). Nuclei were stained with 4', 6-diamidino-2-phenylindole (DAPI; Life Technologies, 1:500-1:1000). After washing, slides were finally mounted with Vectashield (Vector laboratories, #H-1000-10) or Elvanol and imaged using confocal microscopy (Leica SP5, Zeiss LSM880).

Proliferation Analysis

For assessing endocrine cell proliferation, 5-ethynyl-2'-deoxyuridine (EdU) (Thermo, #E-10187) was injected to pregnant *Iir*$^{+/+}$ and *Iir*$^{-/-}$ mice at a dose of 10 mg/g body weight intraperitoneally 2 h prior to sacrifice. Pancreases were dissected from E16.5

and E18.5 embryos and stained for chromogranin-A and EdU as per manufacturer's protocol (Click-IT EdU Alexa Fluor 647 Imaging Kit, Thermo Fisher Scientific). For proliferation analysis in adult control and CKO mice, EdU was added in drinking water (1 mg/mL) for one week prior to sacrifice. DAPI was used to counterstain nuclei (Life Technologies, 1:1000).

Pancreas morphometry and quantification

To evaluate α- and β-cell area in embryonic pancreata, entire pancreas was sectioned at 10 µm thickness and all sections were analysed for insulin and glucagon positive area over total pancreas area. For quantification of EdU and hormone co-positive cells, 4-6 sections per embryo were analysed using IMARIS software. For CKO mice, 10 sections per mice were analysed for insulin and glucagon positive area. The stained tissue sections were scanned with an AxioScan.Z1 digital slide scanner (Zeiss, Jena, Germany) equipped with a 20x magnification objective. The region of interest (islets) were annotated manually and the insulin and glucagon expressing cells were detected. β-cell mass was calculated by multiplying relative insulin-positive area (the percentage of insulin-positive area over total pancreas area) by pancreas weight. To evaluate β-cell replication, the ratio of insulin/EdU/DAPI co-positive cells over the total insulin positive cells were quantified. Images were evaluated using the commercially available image analysis software Definiens Developer XD 2 (Definiens AG, Munich, Germany).

RNA isolation and microarray

Pancreases from embryos (E18.5) or pups (P0) were dissected and stored in RNAlater™ (Ambion #AM7020). RNA extraction was performed using TRIzol reagent (Thermo Fisher Scientific #15596018) and RNeasy Lipid tissue mini kit (Qiagen#74804) according to the manufacturer's protocol. RNA quality and integrity

numbers (RIN) were determined using Agilent 2100 Bioanalyzer (Agilent). RNA samples with RIN > 7 were used for microarray analysis. 30 ng of total RNA was amplified using the Ovation Pico WTA System V2 in combination with the Encore Biotin Module (NuGEN Technologies, Inc, San Carlos, CA, USA). Amplified cDNA was hybridized on a Mouse Transcriptome 1.0 arrays (Affymetrix/Thermo Fisher Scientific, Waltham, USA) and further processed and scanned (Scanner 3000 7G) according to the Affymetrix expression protocol including minor modifications as suggested in the Encore Biotion protocol (NuGENTechnologies,Inc). Expression console (v.1.4.1.46, Affymetrix) was used for quality control and to obtain normalized SST-RMA gene-level data (standard settings including median polish and sketch-quantile normalization). Normalized $\log_2$ expression data were used for subsequent analysis steps, performed in R using Bioconducter packages. Probe sets were annotated using the mta10 transcript cluster.db (v.8.7.0) and filtered (mean $\log_2$ expression value >= 5). Differential expression analysis was performed using limma (v.3.40.2). Functional enrichment analysis was performed on differentially expressed genes (P0 *Iir*$^{-/-}$ vs P0 WT, $p < 0.01$, fold change > 1.5) using Homer (v.4.10). The microarray data have been submitted to GEO (GSE144519). To further validate the microarray results, we carried out quantitative RT-PCR of selected metabolic genes using custom designed Taqman based probe-primer sets (Taqman low density array) (Applied Biosystems) and real time PCR was performed on AB-7500 FAST systems. Data was normalized to housekeeping genes.

Signalling analysis using pancreatic lysate

C-sectioned pubs at E19.5 were starved for 5 h. Pancreata whole-cell lysates were generated. For subsequent Western blot analysis, detection was performed with the following primary antibodies: rat anti-INCEPTOR (14F1, 1:1000); rabbit anti-Igf1r (CST, #9750, 1: 1000); rabbit anti-Insr (CST, #3025, 1: 1000); rabbit anti-Insr/Igf1r-

phospho (CST, #3024, 1:500); mouse anti-Tubulin α (Sigma, #T6199, 1:10,000); rabbit anti-HSP90 (CST, #4874, 1:10,000). Lysis buffers were supplemented with protease inhibitor cocktail (Sigma, #P8340, 1:100), phosphatase inhibitor cocktail 2 (Sigma, #P5726, 1:100) and 3 (Sigma, #P0044, 1:100). Protein concentration of lysates were determined with Pierce™ BCA protein assay kit (Thermo Fisher, #23225). Lysates were resolved on SDS-PAGE, transferred to Immun-Blot PVDF membrane (Biorad, #1620177), blocked in 5% milk for 1 h at RT and incubated with the indicated primary antibodies overnight at 4°C. After washing, membranes were then incubated for 1-2 h at RT with secondary horseradish peroxidase (HRP)-conjugated antibodies (1: 10,000 – 20,000): goat anti-rabbit IgG (Dianova, #111-036-045); goat anti-mouse IgG (Dianova, #115-036-062), rabbit anti-goat IgG (Dianova, #305-035-045). After incubation with Clarity Western ECL Substrate (Biorad, #1705061), bands were detected with ChemStudio2A (Analytik Jena) and densitometric analysis performed with ImageJ.

Intraperitoneal glucose tolerance test (ipGTT) and intraperitoneal glucose stimulated insulin secretion test (ipGSIS)

For ipGTT, mice were fasted for 12 h and injected with glucose (2 g/kg BW, i.p.). Blood glucose was measured at 0, 15, 30, 60 and 120 min post-glucose administration using Contour next glucometer (Bayer). The area under the curve was calculated by the trapezoid rule [$AUC=(C1+ C2)/2\times(t_2-t_1)$]. For ipGSIS, mice were fasted for 12 h and administered with glucose (3 g/kg BW, i.p.). Blood sampling was performed at 0, 2, 5, 15 and 30 min post-glucose administration and quantified for insulin levels using mouse-specific ELISA kits as per manufacturer's guidelines (CrystalChem)

Islet isolation and in vitro assays

Pancreases were excised and digested using collagenase P (Roche, #11213857001) followed by centrifugation using OptiPrep™ density gradient medium (Sigma, #D1556). Isolated islets were handpicked under a stereomicroscope and cultured overnight in RPMI 1640 medium (Invitrogen, #21875091) supplemented with 10% FCS (GIBCO) and 1% penicillin-streptomycin (Life Technologies, 15140122). For *in vitro* islet function tests, islets were induced with tamoxifen (1 µM) or vehicle (EtOH) for 24 h. For Insr/Igf1r signalling, islets were starved for 1h in HEPES-balanced salt solution, stimulated with 100 nM insulin (Novo Nordisk) for the indicated time points and lysed in modified RIPA buffer (150 mM NaCl, 50 mM TRIS-HCl pH 7.4, 1% NP-40, 1 mM EDTA, 0.1% deoxycholate). The following primary antibodies were used: rat anti-INCEPTOR (16F6, 1:1000); rabbit anti-Igf1r (CST, 9750, 1:1000); mouse anti-Insrβ (CST, L6B10, 1:1000); rabbit anti-Insr/Igf1r-phospho (CST, 3024, 1:500); mouse anti-Akt (CST, 2920, 1:1000); rabbit anti-Akt-phospho (S473) (CST, 4060, 1:1000); mouse anti-tubulin γ (Sigma, T5326, 1:10,000); GAPDH (Merck, CB1001, 1:10,000). Islets were isolated from 14 weeks old male CKO mice (MIP-CreERT^{+}; *Iir*$^{fl/FD}$) and treated with (1µM) tamoxifen or vehicle ethanol for 24 h and then labelled with EdU (10 µM) for 72 h.

Protein expression and purification

A gene encoding human *INCEPTOR*-ectodomain (ECD) (KIAA1324, Uniprot entry Q6UXG2, residues 1-910) followed at its C-terminus with 8xHis tag, the human rhinovirus 3C protease cleavage site LEVLFQGP and a tandem-affinity purification tag (Rigaut et al., 1999) was synthesized and cloned into pcDNA3.1 Zeo (+) vector by Genescript. FreeStyle HEK293F cells were transiently transfected with pcDNA3.1-IIR-ECD-8xHis-TAP and the INCEPTOR-ECD was purified as recently described for the human insulin receptor ectodomain[2]. Prior to immunization, affinity purified INCEPTOR

was subjected to size exclusion chromatography using a Superdex 200 Increase 10/300 GL column equilibrated in HBS (50 mM HEPES, 150 mM NaCl, pH 7.5) at a flow rate of 0.5 mL/min at room temperature. Only the top peak fraction of the eluted INCEPTOR-ECD (Extended Data Fig. 4a) was used for poly- and monoclonal anti-INCEPTOR antibody production.

Monoclonal and polyclonal antibody production

Polyclonal rabbit antibodies against the C-terminus of a conserved mouse and human peptide of INCEPTOR (N-TSKRTPDGFDSVPLKT-C) were generated by Pineda Antikörper Service (Berlin) and polyclonal rabbit antibodies against the purified human INCEPTOR ectodomain (1374, 1692) were provided by Coskun Ü. (Paul Langerhans Institute Dresden, Germany). Monoclonal rat antibodies against the INCEPTOR ectodomain (19A6/IgG2b) were generated by immunization with the purified human INCEPTOR ectodomain. Monoclonal rat (EIG14F1/IgG2a; EIG16F6/IgG2b) and mouse (EIG31A11/IgG2b; EIG36D7/IgG2b) antibodies against the cytoplasmic tail of INCEPTOR were generated by immunization of ovalbumin-coupled peptides (N-TSKRTPDGFDSVPLKT-C) of INCEPTOR using standard procedures. All antibodies were validated on Min6 *Iir*$^{+/+}$ and *Iir*$^{-/-}$ cells for specificity by immunocytochemistry, immunohistochemistry and Western blot (1374, 1692-serum, 1:1000; EIG14F1, 16F6, 31A11, 36D7-supernatant, 1:10; Pineda, purified- 1:1000; 19A6, purified, 1:1000).

Cell culture

The murine β-cell line Min6, *Iir*$^{-/-}$ Min6 and INCEPTOR-Venus/INCEPTOR-AP2*-Venus overexpressing Min6 cultured in adherence (2D). Cells were regularly tested negative for mycoplasma (Applichem, #A3744).

Antibody stimulation

For whole cell lysate analysis, Min6 and EndoC-βH1 cells were incubated at 37°C for 5 and 15 min respectively in complete growth medium (DMEM, Thermo Fisher, #11965092) supplemented with rat IgG2b isotype control or 19A6 monoclonal antibody against the ectodomain of INCEPTOR at a final concentration of 1, 5 or 10 µg/mL. Cells were washed 3x with PBS and lysed in RIPA buffer (along with protease and phosphatase inhibitors).

Surface biotinylation assay

For surface biotinylation assays, Min6 and EndoC-βH1 cells were incubated at 37°C for 0, 5, 15 and 30 min at 37°C in growth medium supplemented with a rat antibody against the ectodomain of INCEPTOR (19A6) at a final concentration of 1 µg/mL. Cells were washed 3x with ice-cold PBS (pH 8) and surface proteins were biotinylated with 0.5 mg/mL EZ-Link sulfo-NHS-LC-biotin (Thermo Fisher, #21335) for 30 min at 4°C. Cells were washed 3x with ice-cold PBS (pH 8) followed by quenching of reaction by ice-cold glycine (100 mM, pH 3) for 10 min. Cells were then lysed in mild lysis buffer (2% NP40, 1% TritonX-100, 10% Glycerol, in PBS along with protease and phosphatase inhibitors). Affinity precipitation was performed with Pierce™ Streptavidin magnetic beads (Thermo Fisher, #88817, 1:10) overnight at 4°C under rotation. Beads were washed 3x and eluted with Laemmli-buffer for 5 min at 96°C. For subsequent Western blot analysis, the following primary antibodies were used: rat anti-INCEPTOR (14F1, 1:1000); rabbit anti-Igf1r (CST, #9750, 1:1000); mouse anti-Insrβ (CST, #L6B10, 1:1000); rabbit anti-Insr/Igf1r-phospho (CST, #3024, 1:1000); mouse anti-tubulin γ (Sigma, #T5326, 1:10,000).

Co-immunoprecipitation (co-IP) analysis

For co-IP studies**,** Min6 cells were either maintained under growth conditions, starved for 1 h in HEPES-balanced salt solution (114 mM NaCl, 4.7 mM KCl, 1.2 mM KH_2PO_4, 1.16 mM $MgSO_4$, 20 mM HEPES, 2.5 mM $CaCl_2$, 25.5 mM $NaHCO_3$, pH 7.2) or starved for 1 h followed by stimulation with 100 nM insulin (Recombinant Insulin Human, Novo Nordisk) for 5 and 15 min. Cells were lysed in mild lysis buffer (as described in surface biotinylation assay). Lysate were then added to the Protein G magnetic beads (Sure Beads™, Bio-Rad, #161-4023, 1:10) which were pre-incubated with antibody for 1 h at RT under rotation: Mouse anti-Insrβ (CST, #L6B10, 1:50); rabbit anti-Igf1r (CST, #9750, 1:100); rat anti-INCEPTOR (14F1, 1:100); mouse IgG1 isotype (CST, #5415, 1mg/mL); rabbit IgG isotype (CST, #3900, 1mg/mL); rat IgG isotype (Invitrogen, #9602, 1mg/ml). Beads only control was also added by incubating lysate directly to the non-immobilized beads. Beads were washed gently 3x with lysis buffer and eluted with Laemmli-buffer for 5 min at 96 °C for subsequent Western blot analysis. Detection was performed with the following primary antibodies: rat anti-INCEPTOR (14F1, 1:1000); mouse anti-Insrβ (CST, #L6B10, 1:1000); rabbit anti-Igf1r (CST, #9750, 1:1000); rabbit anti-AP2M1 (abcam, #ab75995, 1:1000); rabbit anti-pAP2M1 (CST, #7399, 1:1000).

CRISPR/Cas9 knock-out in Min6 insulinoma cells

Iir$^{-/-}$ cells were generated by deleting the ATG with two sgRNAs (#1: 5'-*GCATAAGCAGCCACCGCAGC*-3', #2: 5'-*GACAGCGCTATGGCAGAGCC*-3'). Cells were transfected with three plasmids i.e. Cas9-Venus, sgRNA1 and sgRNA2 using Lipofectamine 2000 (Thermo Fisher, #11668027). Cells were then flow sorted for Venus expression 48 h post transfection and seeded in low density for colony formation. Colonies were picked after 1-2 weeks, expanded and genotyped for the deletion.

596 ***Human INCEPTOR constructs***

597 For generating INCEPTOR-Venus, the *INCEPTOR* sequence was amplified from
598 pCMV-KIAA1324[3] using forward primer (5'-
599 *AGTCGGTAGCGGCCGCATGGCTGAGCCTGGGCACAG*-3') and reverse primer (5'-
600 *CTGGACACGCGGCCGCACAGGTCCATGTCTAGGCCTCCT*-3'), digested with *Not*I
601 and ligated into pKS-Venus. After digestion of pKS-*INCEPTOR-Venus* with *Not*I and
602 *Spe*I and pCAG-H2B-Venus with *Not*I and *Nhe*I, products were gel-purified and ligated,
603 generating pCAG-*INCEPTOR-Venus*. For INCEPTOR-AP2*-Venus, pCAG-
604 *INCEPTOR-Venus* was digested with *Asc*I and *Bgl*II and the gel-purified product was
605 ligated with the mutant AP2 binding motif sequence (YSKL to ASKA) by T4 ligase
606 (Thermo Fisher), generating pCAG-*INCEPTOR-AP2*-Venus*. For analysis, stable cell
607 lines were generated by transfecting Min6 cells with the constructs (4 µg DNA) using
608 Lipofectamine 2000 (Thermo Fisher, #11668027) and selecting with 1 µg/mL
609 puromycin (Thermo Fisher, #A1113803) for 3 weeks. Localization of the fluorescent
610 constructs was visualized with a Zeiss LSM 880 confocal microscope. For visualizing
611 plasma membrane CellMask™ Deep Red (Thermo Fisher, #C10046, and 1:2000) was
612 added for 5 min and then fixed in 4% PFA. Quantification was performed using ImageJ
613 by thresholding the plasma membrane stain (red) and measuring fluorescence
614 intensity from the Venus tag (green) at the membrane and throughout the cell.

615

616 ***Subcellular localization***

617 Min6 cells in µ-slide 8 well chambers (Ibidi, #80826) were fixed in 4% PFA for 10 min
618 at RT and permeabilized in 0.25% Triton-X100, 100 mM glycine for 15 min at RT. After
619 blocking in 0.1 % Tween-20, 10 % FCS, 0.1 % BSA and 3 % donkey serum for 1 h at
620 RT, the following primary antibodies were incubated overnight at 4°C: Min6 *Iir*$^{+/+}$, rabbit
621 anti-Tgn46 (Abcam, #ab16059, 1:100); rabbit anti-Rab7 (CST, #9367, 1:100); rabbit

anti-Lamp2 (Thermo Fisher, #PA1-655, 1:300); rabbit anti-clathrin heavy chain (CST, #2410, 1:400); mouse anti-Gm130 (BD, #610822, 1:300); rabbit anti-giantin (BioLegend, #924302, 1:100); rabbit anti-Ergic53 (SCBT, #sc-66880, 1:300); rabbit anti-EEA1 (CST, #2411, 1:300); mouse anti-Cm1 (Coskun Ü., PLID, 1:300); mouse anti-Lamp 1 (Biomol, #VAM-EN001, 1:100) or (BD, #553792, 1:1000). Min6 INCEPTOR-Venus and INCEPTOR-AP2*-Venus, mouse anti-Gm130 (BD, #610822, 1:400), rabbit anti-EEA1 (CST, #2411, 1:200), rabbit anti-giantin (BioLegend, #924302, 1:100), rabbit anti-clathrin heavy chain (CST, #4796, 1:100); mouse anti-INCEPTOR (31A11, supernatant, 1:10). Secondary antibodies were used as described above. Cells were mounted with Elvanol and imaged using Leica SP5 or Zeiss LSM 880 confocal microscope.

Monovalent labelled insulin-AF546

Human insulin (300 mg, 0.052 mmol) was dissolved in H_2O/DMF (60 ml, 2:1) and cooled to 0°C under argon atmosphere. Triethylamine (144 µl, 1.039 mmol) was added to the solution to adjust the pH to 10. A solution of hept-6-ynoic acid NHS ester (10.81 mg, 0.052 mmol) in a mixture of DMF (2.79 ml) and 5% aq. H_2SO_4 (21 µl)) was added gradually in portions of 300 µl. Upon observing the start of formation of disubstituted product, the reaction was stopped by adjusting the pH of the reaction mixture to 3 using 1M aq. hydrochloric acid. The reaction mixture was lyophilised. The lyophilisate was dissolved in a water/acetonitrile mixture (3 ml, 80:20) and purified via HPLC to yield alkyne-modified insulin. **HR-mass:** calculated m/z for $C_{264}H_{391}O_{78}N_{65}S_6$ $(M+3H)^{3+}$ = 1971.5729; found: 1971.5723. A solution of AF546-azide (1.653 mg, 0.02 mmol) in *tert.* butanol (100 µl) was added to a solution of alkyne-modified insulin (6.7 mg, 1.133 µmol) in deionized H_20 (1 ml). A mixture of $CuSO_4$ (0.707 mg, 2.8315 µmol), Tris((1-hydroxy-propyl-1H-1,2,3-triazol-4-yl)methyl)amine (THPTA, 4.927 mg, 0.011 mmol),

sodium ascorbate (4.490 mg, 0.023 mmol) and aminoguanidine hydrochloride (2.506 mg, 0.023 mmol) in H_2O (441 µl) was added to the solution. The solution was allowed to stir for 27 h and the reaction mixture was purified via amicon-15 centrifuge filter units (cut-off 3 kDa). After lyophilisation of the residue, the AF546-labeled insulin (4 mg, 0.581 µmol, 52 %) was obtained as a reddish solid. **HR-mass:** calculated m/z for $C_{304}H_{437}O_{88}N_{71}S_9Cl_3$ $(M+5H)^{5+}$ = 1377.3754; found: 1377.3767.

Insulin uptake assay

Islets were isolated from CKO mice, trypsinized to single cells and treated with tamoxifen for 24 hr followed by a 72 hr wash period. Likewise, Min6 *Iir*$^{+/+}$ and *Iir*$^{-/-}$ cells in µ-slide 8 well chambers (Ibidi, #80826) were starved for 1 h in HEPES-balanced salt solution (114 mM NaCl, 4.7 mM KCl, 1.2 mM KH_2PO_4, 1.16 mM $MgSO_4$, 20 mM HEPES, 2.5 mM $CaCl_2$, 25.5 mM $NaHCO^3$, pH 7.2) and stimulated with 100 nM monovalent insulin-546 (Plettenburg O.) for different time points until fixation in 4% PFA. The cytoskeleton was visualized as SiR-actin (Cytoskeleton, Inc., #CY-SC001, 1:1000) and nuclei with DAPI (Life Technologies, 1:500). Images were captured with a Zeiss LSM 880 microscope and quantified using ImageJ wherein the fluorescent intensity of insulin-546 was divided by the cell number.

Endocytosis assay

Min6 cells grown in µ-slide 8 well chambers (Ibidi, #80826) with 50% confluency were incubated with an ectodomain-specific rabbit anti-INCEPTOR (1374, 1:500) antibody for 30 min at 4°C to prevent endocytosis. After washing 5x with PBS, internalization of the antibody-Inceptor-complex from the surface was chased by further incubation at 37°C for 5, 15, 30 and 60 min until fixation and detected by a secondary donkey anti-rabbit Alexa Fluor® 488 antibody. Primary antibodies for subcellular markers were

incubated overnight at 4°C: mouse anti-Gm130 (BD, 610822, 1:300); mouse anti-Cm1 (Coskun Ü., PLID, 1:300); rabbit anti-Lamp2 (Thermo Fisher, #PA1-655, 1:300). Signal intensity of ecto-Inceptor was enhanced.

Dynasore treatment assay

Localization of the fluorescent constructs was visualized with a Zeiss LSM 880 confocal microscope. For visualizing plasma membrane CellMaskTM Deep Red (Thermo Fisher, #C10046, 1:2000) was added for 5 min and then fixed in 4% PFA. Similarly, the effect of the dynamin inhibitor dynasore (Cayman Chemicals, 14062) was assessed on Min6 cells expressing INCEPTOR-Venus. To this end, cells were seeded on 8 well chambers (ibidi, 80826) and treated with 80 µM dynasore in serum-free DMEM for 2 hours before labeling with CellMask Deep Red and fixation. Quantification was performed using ImageJ by thresholding the plasma membrane stain (red) and measuring fluorescence intensity from the Venus tag (green) at the membrane and throughout the cell.

Proximity ligation assay (PLA)

PLA was performed according to the manufacturer's protocol (Sigma, DuoLink®). Combinations of primary rat/mouse and rabbit antibodies were incubated overnight at 4 °C: rat anti-INCEPTOR (16F6, 1:100-500, detected with anti-mouse PLA probe); rabbit anti-INCEPTOR (Rabbit 3, 1:500) rabbit anti-Insr (Abcam, ab131238, 1:20; rabbit anti-Igf1r (CST, #9750, 1:100), rabbit anti-Igf1r-phospho (SCBT, #sc-101703, 1:100); mouse anti-adaptin β (AP2) (BD, #610382, 1:100). Nuclei were stained with DAPI (Sigma, #D9542, 1:500). Images were acquired as Z-stacks with a Zeiss Axio Observer Z1 epifluorescence microscope using the µManager software and quantified with Image J. After maximum projection, the images of the nuclei were median filtered

and a contrast-limited adaptive histogram equalization was applied. Subsequently, nuclei were segmented and further separated by water shedding. Cell areas were constructed as a Voronoi diagram. The number of PLA dots was counted as the local maxima per cell area using an experiment-dependent noise threshold.

Pearson Correlation Coefficient (PCC)

PCC was calculated using the ImageJ plugin Coloc2 and applying Costes background subtraction to determine the degree of co-localization between Inceptor, INCEPTOR-Venus and INCEPTOR-AP2*-Venus along with different subcellular markers. No correlation, PCC = 0; highest correlation, PCC = 1; highest inverse correlation, PCC = -1.

Bioinformatics analysis

For gene information and domain structure similarities of *Iir*, ensembl.org was used (*5330417C22Rik*). *In-situ hybridization* at E14.5 was obtained from genepaint.org. Amino acid sequences were obtained from UniProt (EIG121, A2AFS3; Insr, P15208; Igf1r, Q60751) and alignments performed with Clustal X2.

Statistical analysis

The results are expressed as means ±SEM (Standard Error Mean) or unless otherwise specified from at least three independent biological experiments. A value of $P<0.05$ was considered statistically significant. All statistical tests, sample size and their *P* values are provided in figure legends description. All statistics were performed using GraphPad Prism software 8 (GraphPad Software Inc., La Jolla, CA).

Reporting summary

Further information on research design is available in the Nature Research Reporting Summary linked to this paper.

Data availability

The microarray data have been deposited in GEO with the accession code GSE144519. Please address correspondence and requests for material to H.L. Source data are provided with this paper.

Extended Data Fig. 1 | Inceptor is expressed in all pancreatic lineages and Inceptor KO embryos showed an increase in endocrine proliferation.

a, *In situ* hybridization showing mRNA expression of *Iir* at embryonic stage E14.5 (genepaint.org).

b, Body weight at postnatal day P0 (Data are mean ± s.e.m.; *P*=0.62; $Iir^{+/+}$, n = 23; $Iir^{-/-}$, n = 11). Significance was calculated using two-tailed, unpaired t-test.

c, Serum glucagon levels after 2-5 h starvation at E19.5 (Data are mean ± s.e.m.; *P*=0.20, $Iir^{+/+}$, n = 8; $Iir^{-/-}$, n = 8). Significance was calculated using a two-tailed, unpaired t-test.

d, α-cell area at E19.5 (Data are mean ± s.e.m.; *P*=0.7906, $Iir^{+/+}$, n = 5; $Iir^{-/-}$, n = 5 mice). Significance were calculated using a two-tailed, unpaired t-test.

e, Confocal images of the expression of Inceptor (green) in endocrine (Ins/Gcg, red/blue), exocrine (amylase, red) and ductal (Sox9, red) cells in the embryonic pancreas at E14.5, E16.5 and E18.5. Scale bar, 50 μm.

f, Confocal images of proliferative (EdU^+, green) endocrine ($ChgA^+$, magenta) cells in *Iir*$^{+/+}$ and *Iir*$^{-/-}$ pancreata at E16.5 (n = 3 mice). White arrow indicates EdU and ChgA co-positive cells. For quantification, see Fig. 1i. Scale bar, 50 µm.

g, Kaplan Meier curve displaying from *Iir*$^{+/+}$, n = 6; *Iir*$^{-/-}$, n = 12 P0 pups after glucose administration. Log rank (Mantel-Cox) test with Welch's t test was performed to compare survival curves (*** $P \leq 0.001$)

h, Blood glucose levels during glucose tolerance test in P0 pups (*Iir*$^{+/+}$, n = 6-12 each time point; *Iir*$^{-/-}$, n = 4-12 each time point). Data are mean ± s.e.m; * $P \leq 0.05$. Significance was calculated by two-way ANOVA followed by Bonferroni's multiple comparisons test.

I, q-PCR of selected genes for microarray validation. Significance was calculated from *Iir*$^{+/+}$ and *Iir*$^{-/-}$ groups (n =4 pups) using multiple t- test. Data are mean ± s.e.m; * $P \leq 0.05$, ** $P \leq 0.01$

Extended Data Fig. 2 │ *Iir* gene structure and protein domains

a-d, Schematic representation of *5330417C22Rik/Iir* gene (a), predicted alternative, protein coding splice variants of *5330417C22Rik/Iir* gene (b), protein domains predicted for the three transcripts of *5330417C22Rik/Iir* gene (c) and various motifs found in the transmembrane domain and cytoplasmic tail of Inceptor (d). Images were modified from ensemble.org

Extended Data Fig. 3 │Domain structure similarities of Inceptor with Insr, Igf1r, CD-M6PR and CI-M6PR/Igf2r

a-b, Amino acid alignment of the first (a) and second (b) predicted cysteine-rich domain (CRD) of Inceptor (aa 272-400 and 574-660, respectively) with the CRD of Insr (aa 180 -336) and Igf1r (aa 169 - 328). Cysteine residues of Insr and Igf1r conserved in Inceptor are indicated in red boxes and non-conserved residues in blue boxes.

c, Amino acid alignment of the mannose-6-phosphate receptor (M6PR) binding domain predicted for Inceptor (aa 654 - 857) with the CD-M6PR (aa 22- 278).

d, Amino acid alignment of the M6PR binding domain predicted for Inceptor (aa 654 - 857) with the 15 repeats of the CI-M6PR/Igf2r. Red box indicates 13 aa with highest similarities (uniprot.org). aa 1897 - 1929 (repeat 13) are not shown.

Amino acids are coloured according to their side chain's chemical properties at pH 7.4: A, F, I, L, M, V, W - hydrophobic (cyan), N, Q, S, T – polar, uncharged (green); R, K – basic (red); C, D, E – acidic (magenta); G (orange), H, Y (blue), P (yellow). "*" indicates single, fully conserved residues. ":" and "." indicate conservation of strong or weak groups according to the Gonnet Pam250 matrix (score > 0.5 or ≤ 0.5, respectively).

Extended Data Fig. 4 | Generation of Iir KO Min6 cell line, production and validation of Inceptor specific mono-/polyclonal antibody.

a, Affinity purified human INCEPTOR ectodomain from human embryonic kidney cells (HEK293F) showing size exclusion chromatography purified INCEPTOR protein and its validation on SDS-PAGE.

b, Schematic representation of the CRISPR/Cas9 targeting strategy for the generation of Min6 *Iir*$^{-/-}$ cells. Min6 cells were transfected followed by FACS sorting

of Venus positive cells and colonies were picked for genotyping. Two sgRNAs were used to delete the start codon from exon 1.

c, Schematic representation of INCEPTOR domains and an indication of antibodies generated against either extracellular domain or cytoplasmic domain.

d, Immunostaining in Min6 *Iir*$^{+/+}$ and *Iir*$^{-/-}$ cells using the mouse (31A11, 36D7), rat (14F1, 16F6) and rabbit (1374, 1692) anti-Inceptor (green) antibodies. Scale bar, 10 µm.

e, Immunostaining in the pancreata of E19.5 embryo from *Iir*$^{+/+}$ and *Iir*$^{-/-}$ mice using rat (19A6) and rabbit (1374) anti-Inceptor (green) antibodies. Scale bar, 50 µm

f, Immunostaining using rat (16F6) and rabbit (1374) anti-Inceptor (green) antibodies in adult mouse pancreas (6 months old). Scale bar, 50 µm

g Validation of mouse/rat/rabbit anti-Inceptor antibodies in Min6 *Iir*$^{+/+}$ and *Iir*$^{-/-}$ cells by Western blot analysis.

Extended Data Fig. 5 | Generation of full body Inceptor KO and β-cell specific conditional knock-out (CKO) mice.

a, Schematic representation of the targeted *Iir* allele for the generation of full-body KO (*Iir*$^{-/-}$) and CKO (MIP-CreERT+;Iir$^{flox/FD}$) mice.

b-c, Genotyping of full body KO (*Iir*$^{+/+}$, *Iir*$^{+/-}$, *Iir*$^{-/-}$) (b), control and CKO animals (*Iir*$^{flox/+}$ and *Iir*$^{flox/FD}$) (c) in combination with MIP-CreERT^{+} and MIP-CreERT^{-}).

d, Mating scheme for the generation of CKO and control animals. To rule out the effects of MIP-CreERT allele and tamoxifen, we used these two indicated F1 genotypes.

e-f, Body weight (e) and α-cell mass (f) in control (n=12 and 3, respectively) and CKO (n=14 and 4, respectively) male mice, 4 weeks post tamoxifen injection. Data are mean ± s.e.m. No significant changes were observed.

g, Experimental paradigm showing *in vitro* tamoxifen-induced gene deletion in isolated islets. Islets were isolated from 14-week old male CKO mice and induced with tamoxifen (1μM) or vehicle (ethanol) for 24 h and followed by 72 h wash period. EdU (10 μM) was added to the culture media during the wash period to label replicating cells. Islets were then fixed and immunostained for insulin and EdU co-positive cells. For signalling assays, islets were induced with 100 nM insulin for 15 mins. Immunostaining (left penal) showing *in vitro* deletion efficiency of Iir (green) in β-cells of male CKO mice. EtOH injection served as control. Islet area is indicated in white dashed outline. Scale bar, 50 μm. Immunostaining (right penal) showing the proliferation (EdU, green) in β-cells (insulin, magenta) of CKO mice islets. Islets from 14 weeks old male MIP-CreERT+; $Iir^{flox/FD}$ mice were induced with either tamoxifen (1 μM) or ethanol to rule out the effect of MIP-CreERT on proliferation. Scale bar, 50 μm.

h, Iir immunoreactivity in the hypothalamus at the level of the arcuate nucleus (A) and paraventricular nucleus (B) in WT and CKO mice. ARH = Arcuate nucleus, VMH = Ventromedial nucleus, DMH = Dorsomedial nucleus, PVH = Paraventricular nucleus, 3V = Third ventricle. Scale bar = 200 μm.

i, Immunostaining for maturation markers UCN3 and MafA from control and CKO mice pancreas. Scale bar = 50 μm (UCN3), 20 μm (MafA)

Extended Data Fig. 6 | Inceptor routes in the secretory pathway and is quickly internalized to the Golgi-ER-lysosomes

a, Representative confocal images demonstrating co-localization of Inceptor (green) with giantin, CM1, Eea1, GM130, ERGIC53, or Lamp1 (magenta) and quantified by Pearson correlation coefficient (n = 3; giantin, 300; Cm1, 296; Eea1, 202; GM130, 350; ERGIC53, 257; Lamp1, 273 cells in total). Scale bar, 10 μm.

b-e, Experimental design (b) for the endocytosis assay of Inceptor. Representative confocal images (c) and quantification by Pearson correlation coefficience (d) of the internalization of Inceptor (green) from the plasma membrane within COP-vesicles (CM1, magenta) or to lysosomes (Lamp2, magenta) at different time points. Within 10-30 min, Inceptor was also found to a higher extent in lysosomes and COP vesicles. (CM1, n = 4, 1225; Lamp2, n = 3, 766 cells in total). No antibody and pre-immune serum (e) served as control. Scale bar, 10 μm.

f, Representative confocal images of the co-localization of INCEPTOR-Venus (green) with endogenous Inceptor, Gm130, giantin, EEA1 or clathrin (magenta) quantified as Pearson's correlation coefficient (*n* = 3; Gm130 -111 cells/n, 383 cells in total; giantin -100 cells/n, 329 cells in total; EEA1 -107 cells/n, 332 cells in total; clathrin, -80 cells/n, 495 cells in total). Scale bar, 10 μm.

g, Representative confocal images of the co-localization of INCEPTOR-AP2*-Venus (green) with Gm130 or clathrin (magenta) quantified as Pearson's correlation coefficient (*n* = 3; Gm130 -63 cells/n, 220 cells in total; clathrin, -136 cells/n, 432 cells in total). Scale bar, 10 μm.

Extended Data Fig. 7 | Interaction of Inceptor with Insr/Igf1r and reduced uptake of labelled insulin in *lir*knock out Min6 cells and mouse islets.

a-b, Interaction of endogenous Inceptor with Insr in WT mouse islets (5 months old mice) when co-immunoprecipitated using an anti-Insr antibody under different metabolic conditions. Beads only and IgG served as IP-controls. Box and whisker plots (min to max) showing relative density (fold change) of proteins (n=3; biologically independent samples data are mean ± s.e.m. * $P \leq 0.05$, ** $P \leq 0.01$, *** $P \leq 0.001$). Significance was calculated using one-way ANOVA followed by Bonferroni's multiple comparisons test.

c, Proximity ligation assay for endogenous Inceptor alone as well as together with Insr, Igf1r and p-Igf1r in Min6 $Iir^{-/-}$ cells. Scale bar, 50 µm

d, Immunostaining showing the uptake of insulin-546 by Insr/Igf1r at different time points in Min6 $Iir^{+/+}$ and $Iir^{-/-}$ cells. For quantification see Fig. 4 e. Scale bar, 10 µm.

e-f, Immunostaining showing the uptake of insulin-546 by Insr/Igf1r at different time points in control and CKO mouse dispersed islets treated with tamoxifen (1 µM for 24 h). Live cell imaging was performed at different time points. Scale bar, 100 µm. (~200 cells were quantified; data are mean ± s.e.m. * $P \leq 0.05$, ** $P \leq 0.01$, *** $P \leq 0.001$). Significance was calculated using two-way ANOVA followed by Bonferroni's multiple comparisons test.

g, Western blot images of the input for the surface biotinylation assay as shown in Fig. 4 h-i.

Extended Data Fig. 8 | Inceptor directly interacts with pAP2M1 and regulates AP2-mediated endocytosis of InsR/IGF1R.

a-b, Immunostaining showing the effect of CME inhibitor (Dynasore) on Inceptor endocytosis. INCEPTOR-Venus expressing cells were treated with 80 μM Dynasore in serum-free DMEM for 2 h before labeling with CellMask Deep Red and fixation. Analysis was performed by quantifying the ratio of INCEPTOR-Venus (green) in the membrane (red) v/s intracellular region. n=3; biologically independent experiment; data are mean ± s.e.m. * $P \leq 0.05$, ** $P \leq 0.01$, *** $P \leq 0.001$). Significance was calculated using unpaired t-test. Scale bar, 10 μm

c-e, Interaction of endogenous Incpetor and INCEPTOR-Venus with p-AP2M1 in Min6 cells when co-immunoprecipitated using an anti-INCEPTOR ectodomain antibody under different metabolic conditions. Mutation in AP2-binding motif in INCEPTOR-AP2* Venus fails to interact with p-AP2M1 subunit. Beads only and IgGs served as IP-controls. (n=3; biologically independent experiment;data are mean ± s.e.m. * $P \leq 0.05$, ** $P \leq 0.01$, *** $P \leq 0.001$). Significance was calculated using two-way ANOVA followed by Bonferroni's multiple comparisons test.

f-i, Western blot analysis and quantification from Min6 cells expressing endogenous Inceptor, INCEPTOR-Venus WT and INCEPTOR-AP2*-Venus overexpression under different metabolic conditions. (n=3; biologically independent experiment; data are mean ± s.e.m. * $P \leq 0.05$, ** $P \leq 0.01$, *** $P \leq 0.001$). Significance was calculated using two-way ANOVA followed by Bonferroni's multiple comparisons test.

Extended Data Fig. 9 | Effect of INCEPTOR monoclonal antibody on human EndoC-βH1 cell line.

a-b, Western blot analysis and quantification from EndoC-βH1 cells under growth conditions treated with rat anti-INCEPTOR mAb and IgG2b (control) for 15 min at three different concentrations. (*n* = 3; biologically independent experiment; data are mean ± s.e.m. * *P*≤0.05, ** *P*≤0.01, *** *P*≤0.001). Significance was calculated using a two-way ANOVA followed by Bonferroni's multiple comparisons test.

c-d, Surface biotinylation assay showing surface pools of INCEPTOR, p-Insr/Igf1r, Insr and Igf1r in EndoC-βH1 cells treated with rat anti-INCEPTOR mAb (1μg/mL) at different time points compared to IgG2b control. Quantification of the surface pools at different time points. (*n* = 3; biologically independent experiment; data are mean ± s.e.m. * *P*≤0.05, ** *P*≤0.01, *** *P*≤0.001). Significance was calculated using a two-way ANOVA followed by Bonferroni's multiple comparisons test.

Acknowledgements: We are grateful to Mostafa Bakhti, Elke Schlüssel, Anika Böttcher and Mara Catani for comments and discussions. We thankfully acknowledge Robert Fimmen, Jürgen Schultheiß, Julia Beckenbauer and Lisa Appel for their great technical support. We are thankful for the Min6 K8 and K20 clones from Jun-ichi Miyazaki from Osaka University and the EndoC-βH1 cells from Raphael Scharfman. This work was supported by funds from the Helmholtz future topic "Aging and Metabolic programming" (AMPro) the Helmholtz Society, Helmholtz Portfolio Theme 'Metabolic Dysfunction and Common Disease, German Research Foundation and German Center for Diabetes Research (DZD e.V.). F.F.F. was kindly supported by a PhD fellowship from the Hans-Seidl Stiftung e.V.

Author Information:

Affiliations

Institute of Diabetes and Regeneration Research, Helmholtz Center Munich, Neuherberg, Germany

Ansarullah, Chirag Jain, Fataneh Fathi Far, Katharina Wißmiller, Sarah Homberg, Felizitas Gräfin von Hahn, Aurelia Raducanu, Silvia Schirge, Michael Sterr, Sara Bilekova, Johanna Siehler, Lena Oppenländer, Amir Morshedi, Aimée Bastidas-Ponce & Heiko Lickert

Institute of Bioengineering and Microfluidics, Helmholtz Center Munich, Neuherberg, Germany

Matthias Meier & Julius Wiener

Institute of Experimental Genetics, Helmholtz Center Munich, Neuherberg, Germany

Martin Irmler & Johannes Beckers

Institute of Diabetes and Obesity, Helmholtz Center Munich, Neuherberg, Germany

Gustav Collden, Timo D. Müller & Matthias H. Tschöp

Core Facility Pathology and Tissue Analytics, Helmholtz Center Munich, Neuherberg, Germany

Annette Feuchtinger

Monoclonal Antibody Core Facility, Helmholtz Center Munich, Neuherberg, Germany

Regina Feederle

Institute for Medicinal Chemistry, Helmholtz Center Munich, Neuherberg, Germany

Christin Ahlbrecht & Oliver Plettenburg

Institute of Organic Chemistry, Center of Biomolecular Research, Leibniz Universität Hannover, Hannover, Germany

Christin Ahlbrecht & Oliver Plettenburg

Technical University of Munich, School of Medicine, Munich, Germany

Fataneh Fathi Far, Katharina Wißmiller, Sarah Homberg, Felizitas Gräfin von Hahn, Michael Sterr, Sara Bilekova, Johanna Siehler, Lene Oppenländer, Aimée Bastidas-Ponce, Martin Irmler, Johannes Beckers & Heiko Lickert

Chair of Experimental Genetics, School of Life Sciences Weihenstephan, Technische Universität München, Freising, Germany

Johannes Beckers

Paul Langerhans Institute Dresden of Helmholtz Center Munich, Technical University Dresden, Dresden, Germany

Michal Grzybek & Ünal Coskun

German Center for Diabetes Research (DZD), Neuherberg, Germany

Ansarullah, Chirag Jain, Aurelia Raducanu, Silvia Schirge, Michael Sterr, Aimée Bastidas-Ponce, Martin Irmler, Johannes Beckers, Michal Grzybek, Oliver Plettenburg, Christin Ahlbrecht, Timo D. Müller, Matthias H. Tschöp, Ünal Coskun & Heiko Lickert

Contributions: A., C.J., F.F.F., K.W., S.H., F.G.H., A.R., S.S., S.B., J.S., J.W., L.O., A.M, A.B.P., G.C., A.F. and M.G. performed experiments and analysed the data. M.S., M.I. and J.B. performed and analysed microarray experiments. C.A and O.P. generated monovalent labelled insulin. Ü.C. provided all polyclonal antibodies against the complete INCEPTOR ectodomain. R.F. generated all monoclonal anti-INCEPTOR peptide antibodies. R.F. and Ü.C. generated monoclonal antibodies against the complete INCEPTOR ectodomain and M.G. performed biochemical validation experiments thereof. T.D.M., M.M., Ü.C., M.H.T. and H.L. supervised the study and A., C.J., S.H. and H.L. prepared the manuscript. H.L. conceived and designed the study, supervised the work and secured funding.

Corresponding author:

Correspondence to heiko.lickert@helmholtz-muenchen.de

Ethics declaration:

Competing interests:

Helmholtz Zentrum München owns a patent (WO2017042242), 'Novel IGFR-LIKE RECEPTOR AND USES THEREOF', covering the targeting of INCEPTOR for diabetes therapy.

References: (19 References)

1 Kulkarni, R. N. *et al.* Tissue-specific knockout of the insulin receptor in pancreatic beta cells creates an insulin secretory defect similar to that in type 2 diabetes. *Cell* **96**, 329-339, doi:10.1016/s0092-8674(00)80546-2 (1999).

2 Ueki, K. *et al.* Total insulin and IGF-I resistance in pancreatic beta cells causes overt diabetes. *Nat Genet* **38**, 583-588, doi:10.1038/ng1787 (2006).

3 Goldfine, A. B. & Kulkarni, R. N. Modulation of beta-cell function: a translational journey from the bench to the bedside. *Diabetes Obes Metab* **14 Suppl 3**, 152-160, doi:10.1111/j.1463-1326.2012.01647.x (2012).

4 Lemmon, M. A. & Schlessinger, J. Cell signaling by receptor tyrosine kinases. *Cell* **141**, 1117-1134, doi:10.1016/j.cell.2010.06.011 (2010).

5 Ghosh, P., Dahms, N. M. & Kornfeld, S. Mannose 6-phosphate receptors: new twists in the tale. *Nat Rev Mol Cell Biol* **4**, 202-212, doi:10.1038/nrm1050 (2003).

6 Okada, T. *et al.* Insulin receptors in beta-cells are critical for islet compensatory growth response to insulin resistance. *Proc Natl Acad Sci U S A* **104**, 8977-8982, doi:10.1073/pnas.0608703104 (2007).

7 Kulkarni, R. N. *et al.* beta-cell-specific deletion of the Igf1 receptor leads to hyperinsulinemia and glucose intolerance but does not alter beta-cell mass. *Nat Genet* **31**, 111-115, doi:10.1038/ng872 (2002).

8 Kulkarni, R. N. *et al.* Impact of genetic background on development of hyperinsulinemia and diabetes in insulin receptor/insulin receptor substrate-1 double heterozygous mice. *Diabetes* **52**, 1528-1534, doi:10.2337/diabetes.52.6.1528 (2003).

9 Mehran, A. E. *et al.* Hyperinsulinemia drives diet-induced obesity independently of brain insulin production. *Cell Metab* **16**, 723-737, doi:10.1016/j.cmet.2012.10.019 (2012).

10 Belfiore, A. & Malaguarnera, R. Insulin receptor and cancer. *Endocr Relat Cancer* **18**, R125-147, doi:10.1530/ERC-11-0074 (2011).

11 Boucher, J., Kleinridders, A. & Kahn, C. R. Insulin receptor signaling in normal and insulin-resistant states. *Cold Spring Harb Perspect Biol* **6**, doi:10.1101/cshperspect.a009191 (2014).

12 Goh, L. K. & Sorkin, A. Endocytosis of receptor tyrosine kinases. *Cold Spring Harb Perspect Biol* **5**, a017459, doi:10.1101/cshperspect.a017459 (2013).

13 Choi E, Zhang X, Xing C, Hongtao Y. Checkpoint regulators control insulin signaling and metabolic homeostasis. *Cell* 166, 1-15 (2016).

14 Choi, E. *et al.* Mitotic regulators and the SHP2-MAPK pathway promote IR endocytosis and feedback regulation of insulin signaling. *Nat Commun* **10**, 1473, doi:10.1038/s41467-019-09318-3 (2019).

15 Rhodes, C. J., White, M. F., Leahy, J. L. & Kahn, S. E. Direct autocrine action of insulin on beta-cells: does it make physiological sense? *Diabetes* **62**, 2157-2163, doi:10.2337/db13-0246 (2013).

16 Zick, Y. Ser/Thr phosphorylation of IRS proteins: a molecular basis for insulin resistance. *Science's STKE : signal transduction knowledge environment* **2005**, pe4, doi:10.1126/stke.2682005pe4 (2005).

17 Wang, M., Li, J., Lim, G. E. & Johnson, J. D. Is dynamic autocrine insulin signaling possible? A mathematical model predicts picomolar concentrations of extracellular monomeric insulin within human pancreatic islets. *PLoS One* **8**, e64860, doi:10.1371/journal.pone.0064860 (2013).

18 Bauer, M., Aust, G. & Schumacher, U. Different transcriptional expression of KIAA1324 and its splicing variants in human carcinoma cell lines with different metastatic capacity. *Oncol Rep* **11**, 677-680 (2004).

19 Deng, L. *et al.* Identification of a novel estrogen-regulated gene, EIG121, induced by hormone replacement therapy and differentially expressed in type I

and type II endometrial cancer. *Clin Cancer Res* **11**, 8258-8264, doi:10.1158/1078-0432.CCR-05-1189 (2005).

References for methods part:

20. Tamarina, N. A., Roe, M. W. & Philipson, L. Characterization of mice expressing Ins1 gene promoter driven CreERT recombinase for conditional gene deletion in pancreatic beta-cells. *Islets* **6**, e27685, doi:10.4161/isl.27685 (2014).
21. Gutmann, T., Schäfer, I.B., Poojari, C., Brankatschk, B., Vattulainen, I., Strauss, M. & Coskun, Ü. Cryo-EM structure of the complete and ligand-saturated insulin receptor ectodomain. *J Cel Biol* **219(1)**. doi: 10.1083/jcb.201907210
22. Kang, J. M. *et al.* KIAA1324 Suppresses Gastric Cancer Progression by Inhibiting the Oncoprotein GRP78. *Cancer Res* **75**, 3087-3097, doi:10.1158/0008-5472.CAN-14-3751 (2015).

Fig. 1 | Inceptor is highly expressed in the pancreas, regulates endocrine cell proliferation and Ins/Igf1 signalling

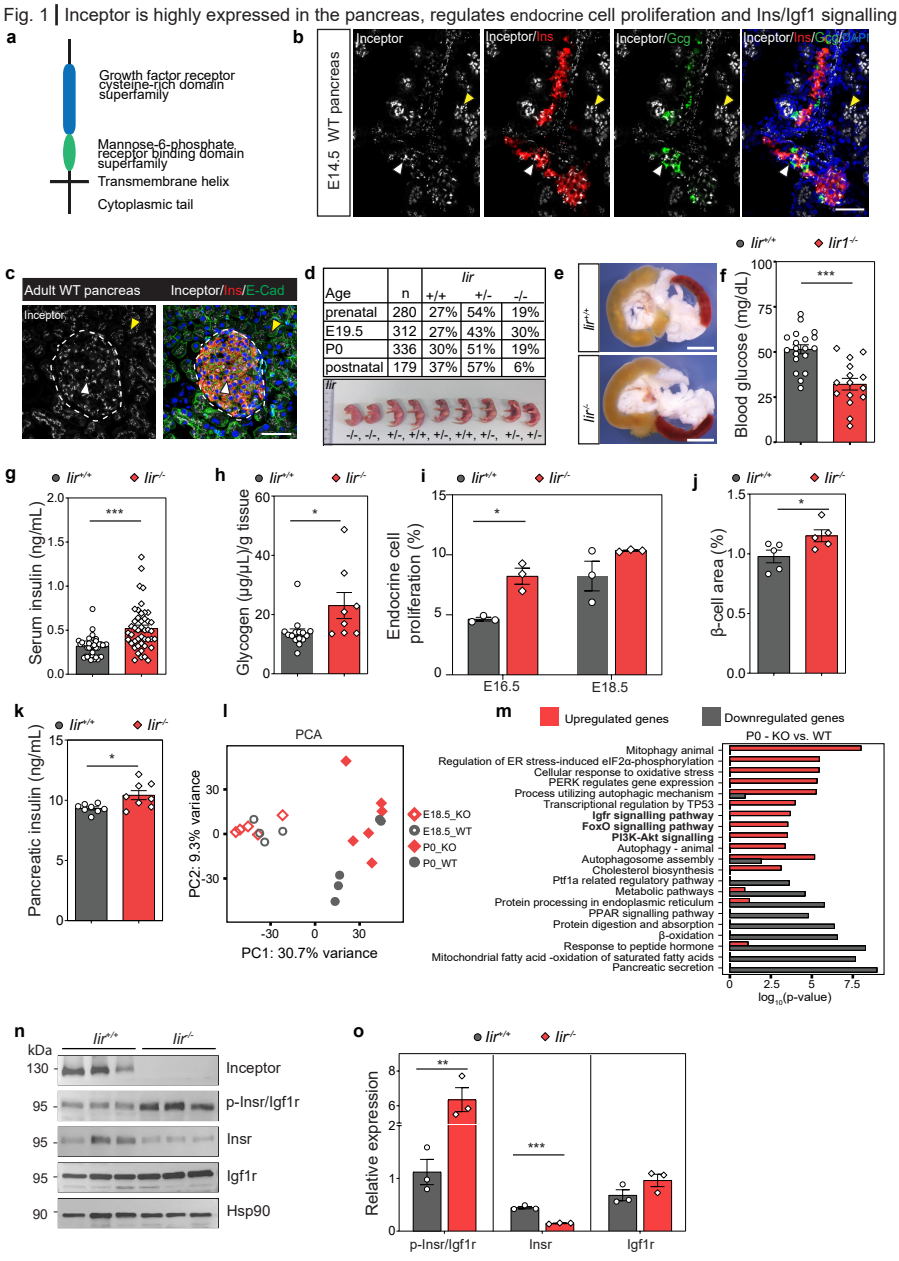

Fig. 2 | Tamoxifen-inducible β-cell specific knock-out of *Iir* causes increased Insr/Igf1r signalling and β-cell proliferation leading to improved glucose tolerance

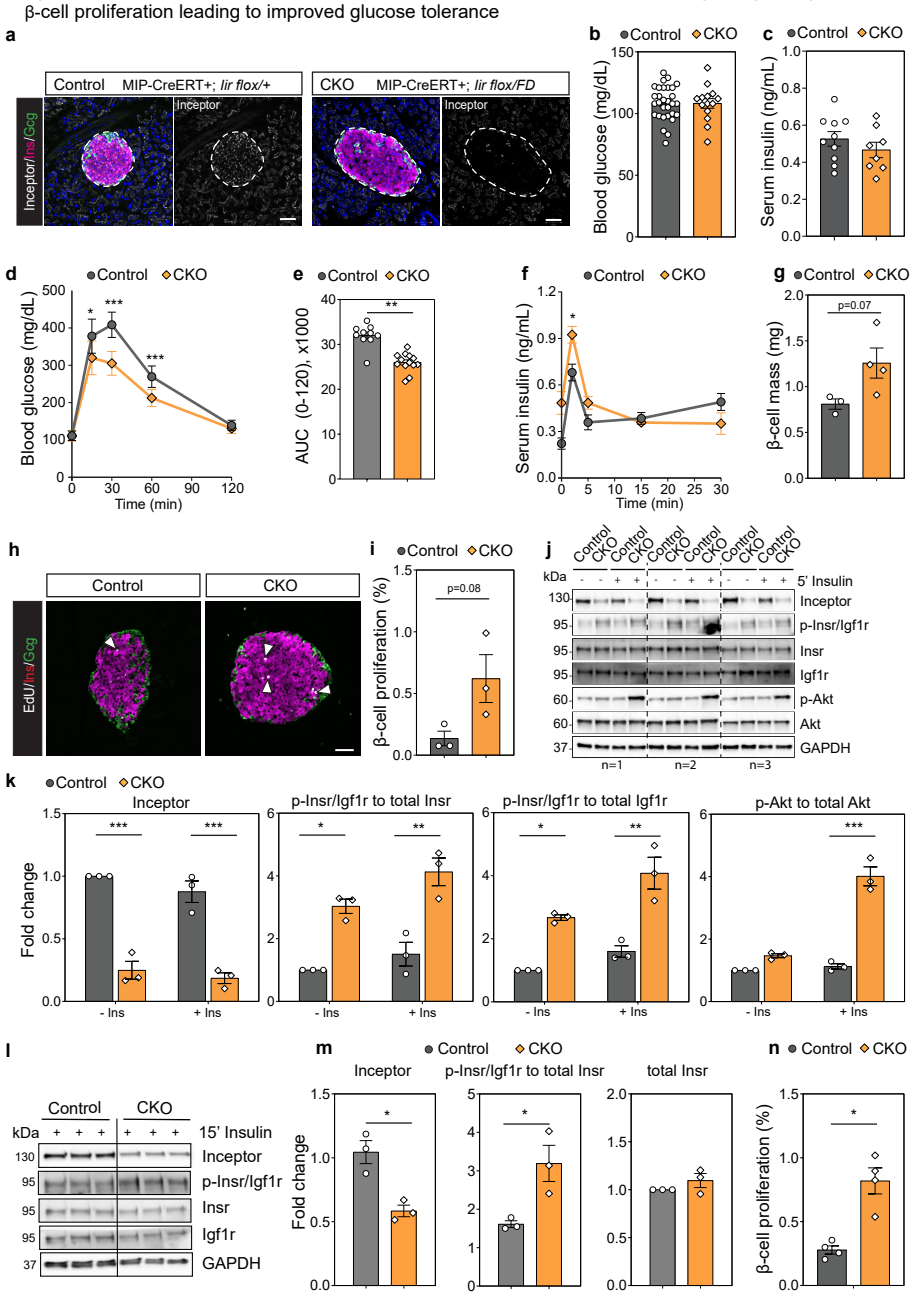

Fig. 3 | Inceptor is mainly localized in the Golgi-ER-lysosomal compartment and internalized via clathrin-mediated endocytosis

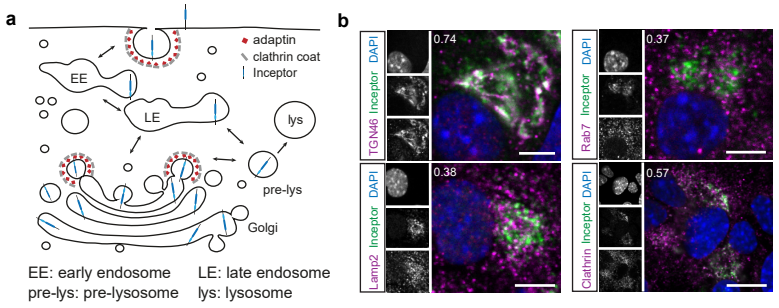

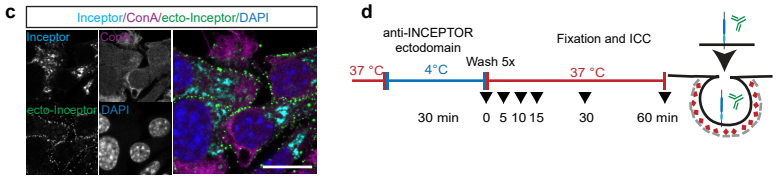

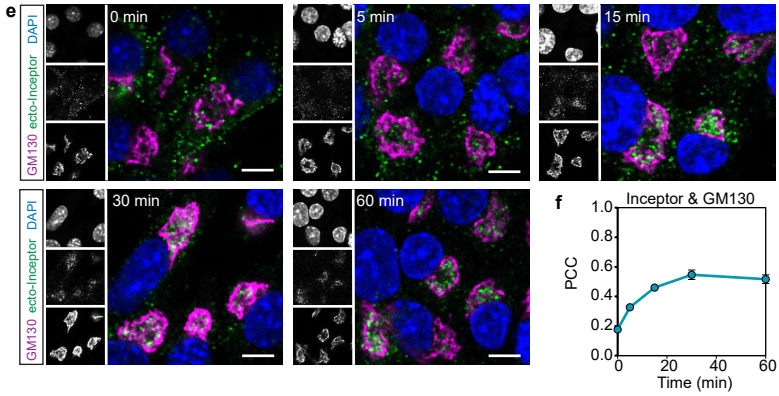

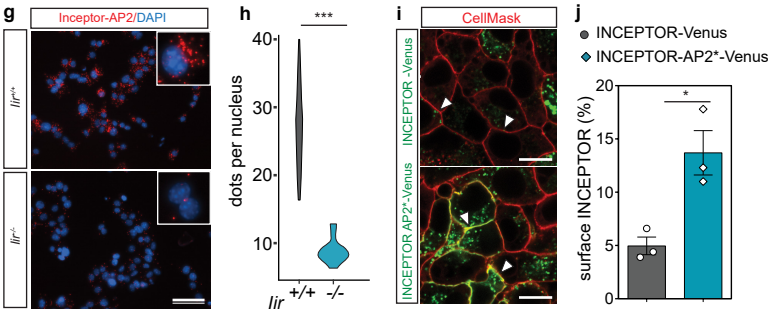

Fig.4 | Inceptor physically interacts with Insr and Igf1r to enhance receptor internalization and densensitization

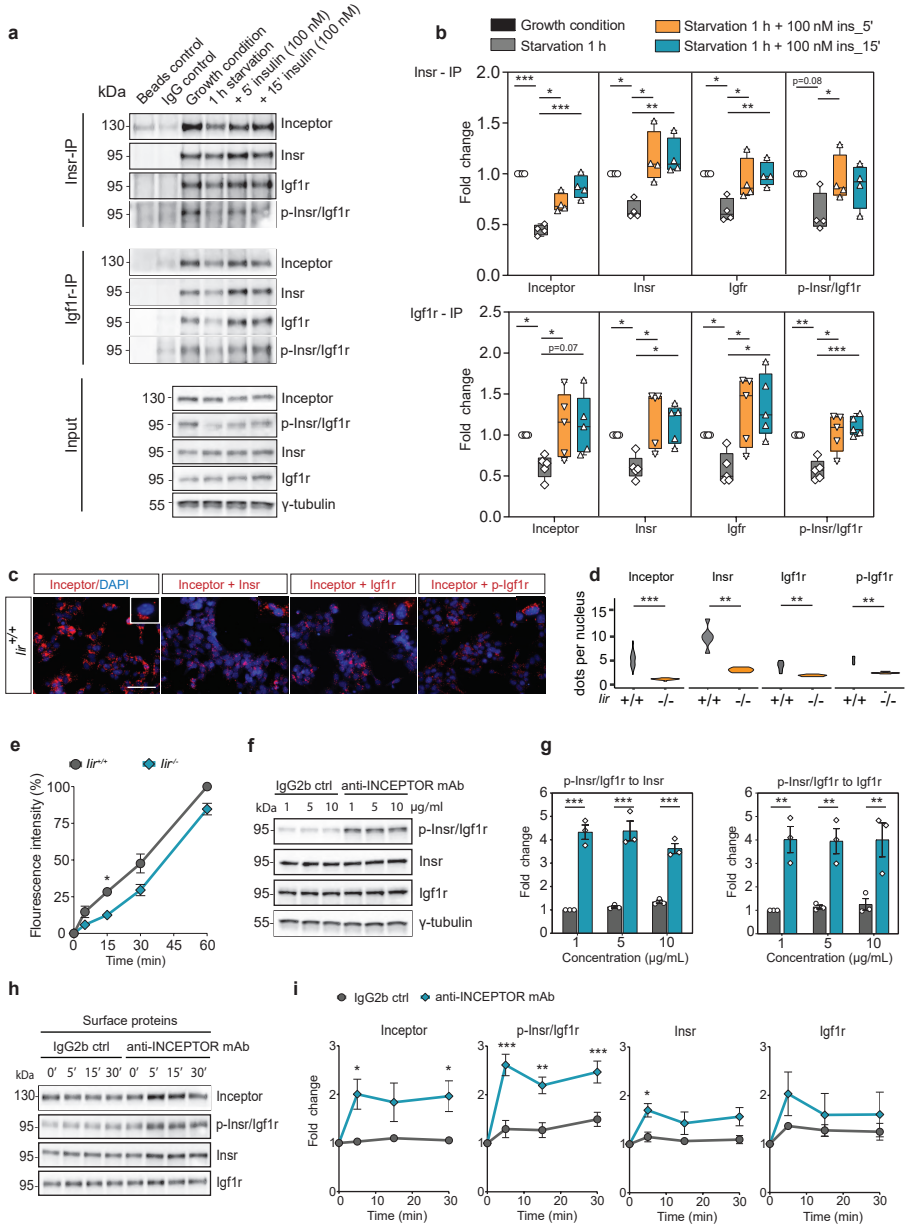

Extended Data Fig. 1 | Inceptor is expressed in all pancreatic lineages and *Iir* KO embryos showed an increase in endocrine proliferation

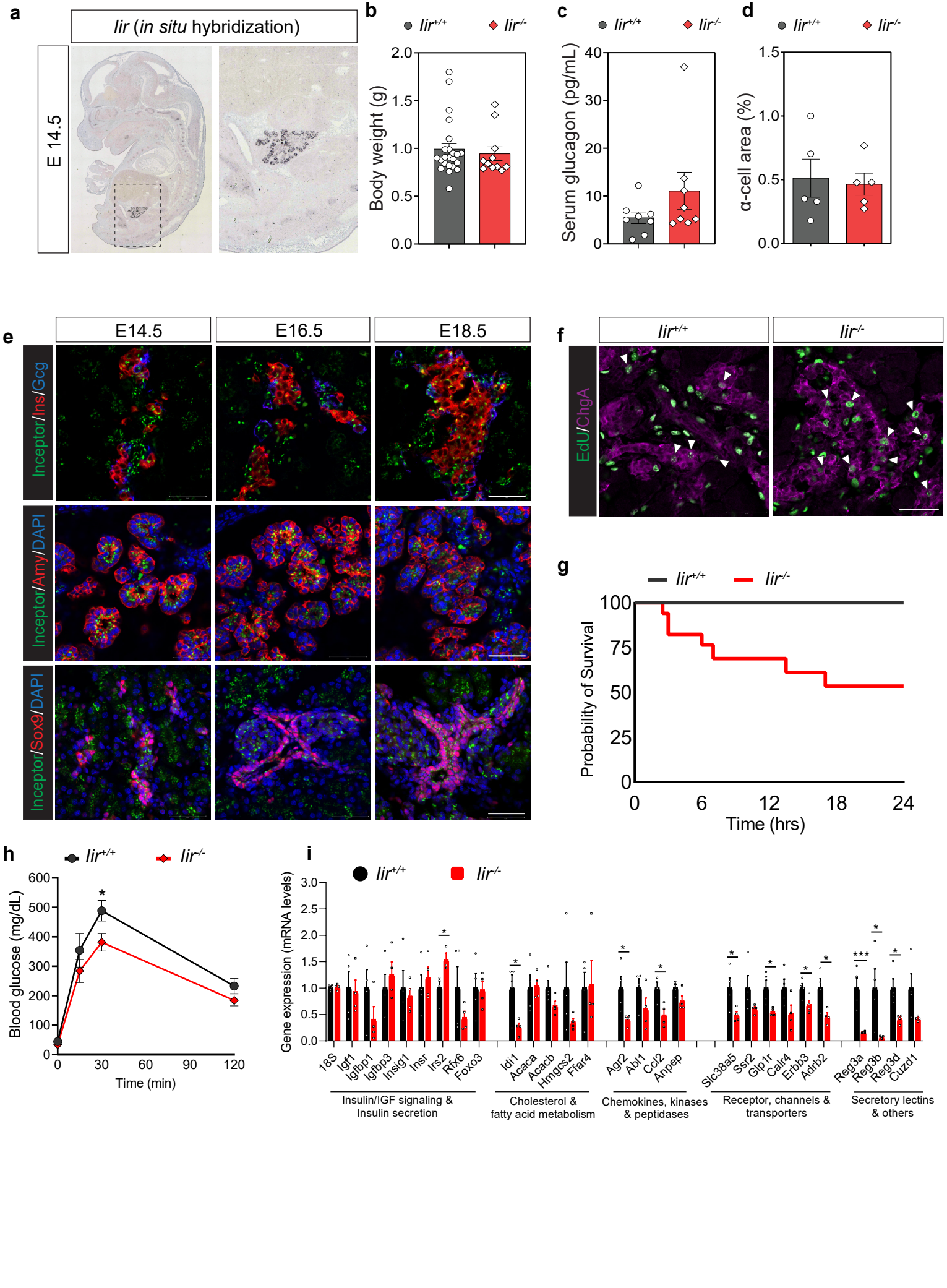

Extended Data Fig. 2 | Domain structure similarities of Iir with Insr, Igf1r, CD-M6PR and CI-M6PR/Igf2r

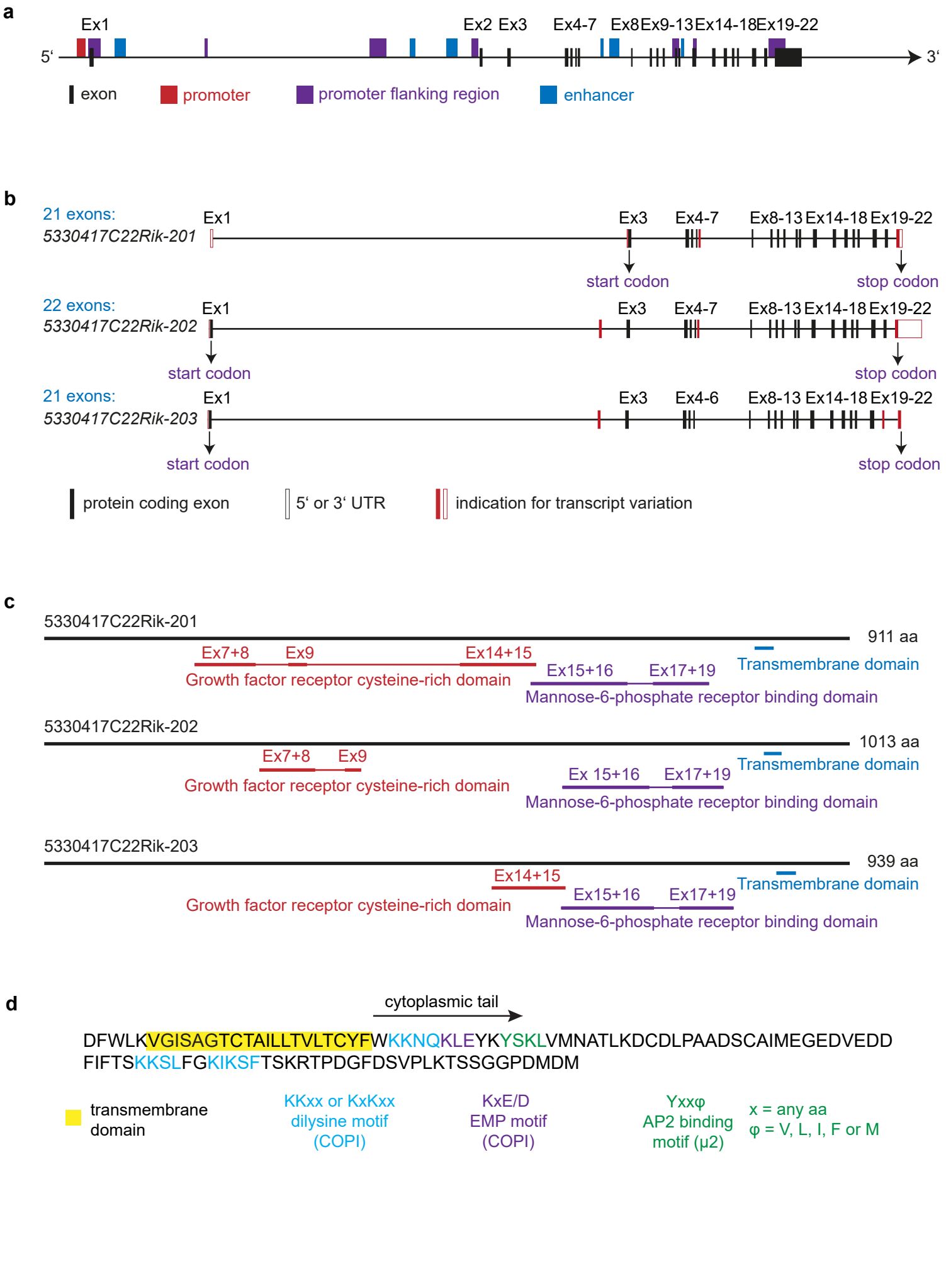

Extended Data Fig. 3 | Domain structure similarities of Inceptor with Insr, Igf1r, CD-M6PR and CI-M6PR/Igf2r

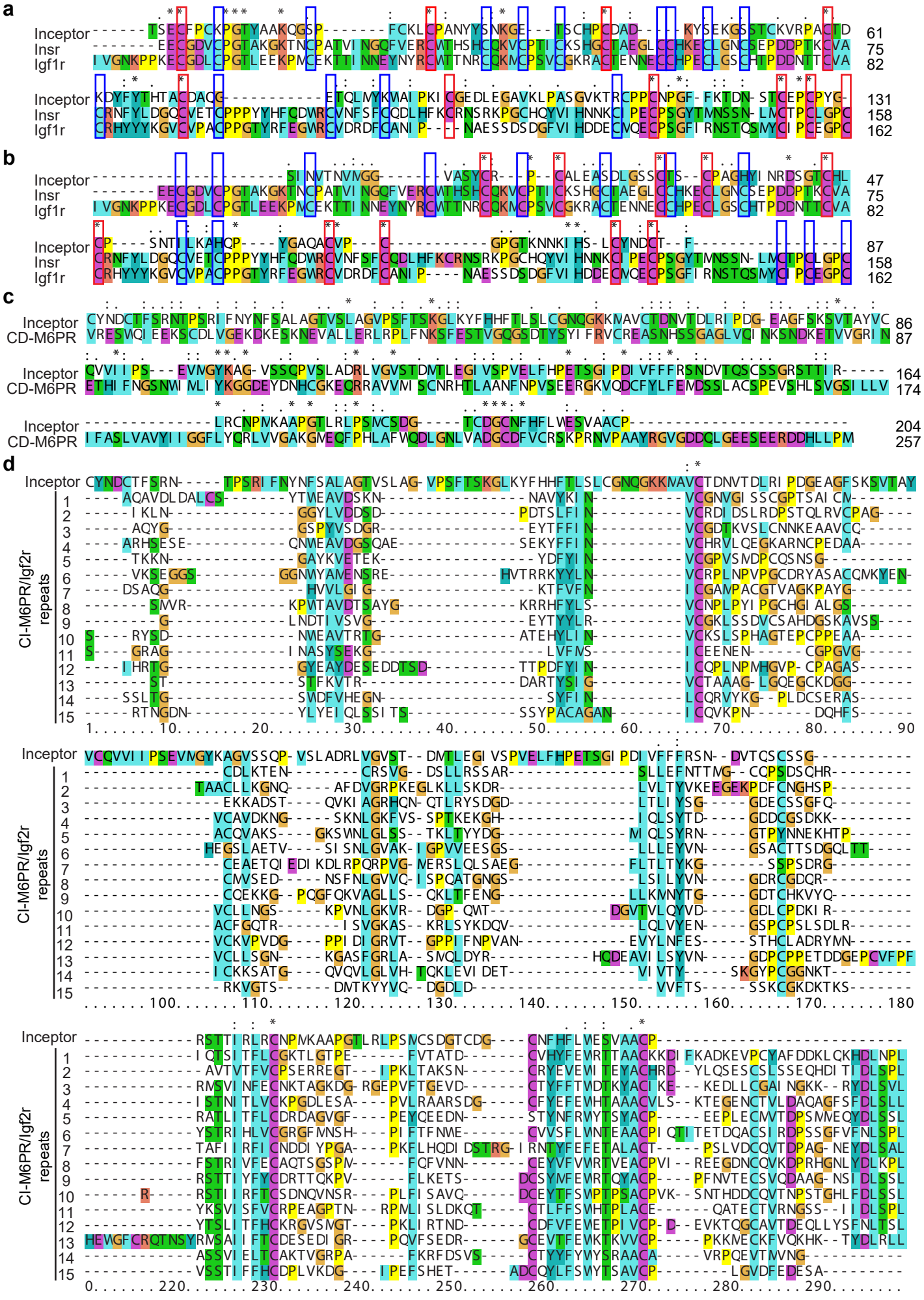

Extended Data Fig. 4 | Generation of *lir* knock out in Min6 cell line, production and validation of INCEPTOR specific mono/polyclonal antibodies

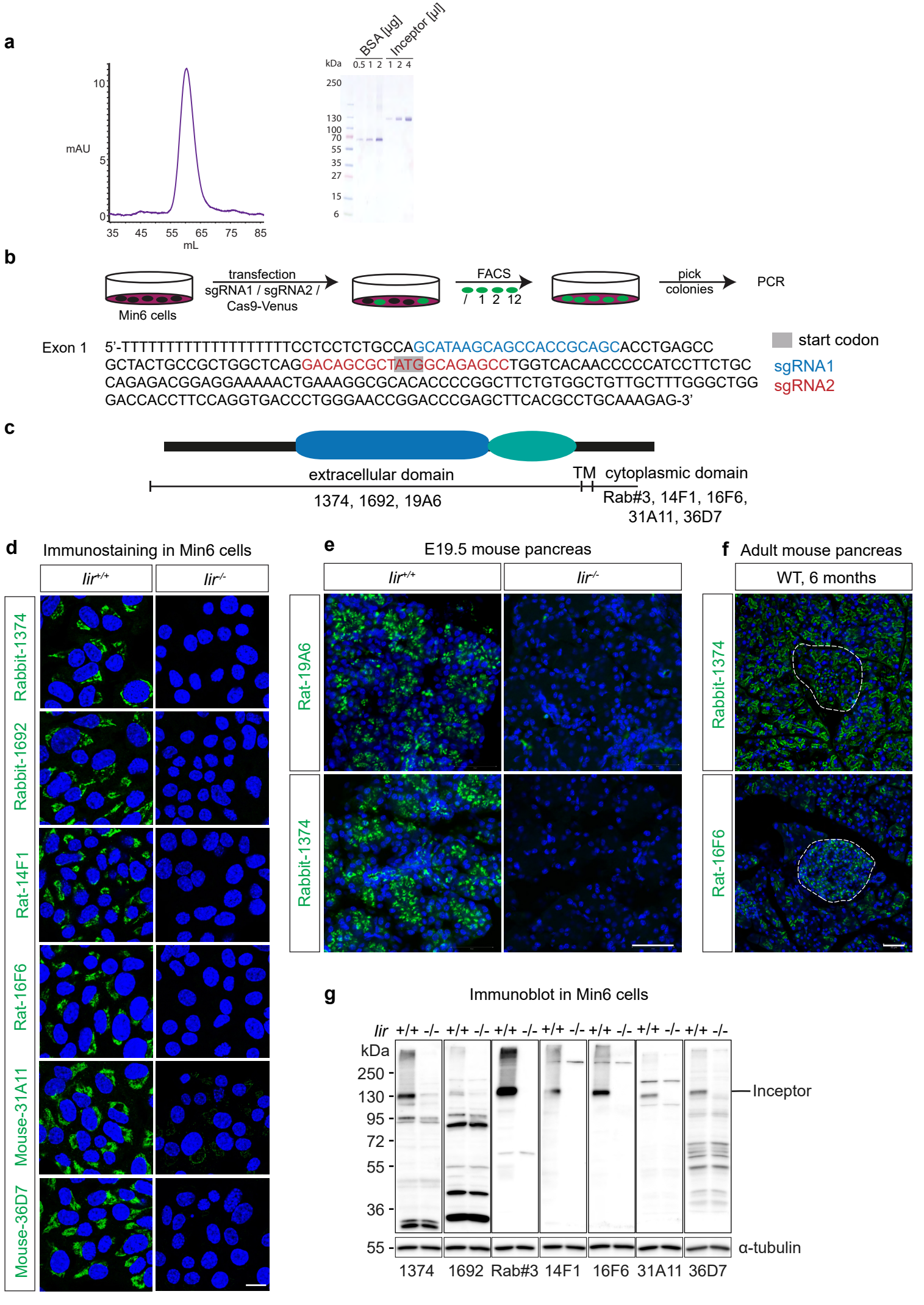

Extended Data Fig. 5 | Generation of full body *lir*$^{-/-}$ and β-cell specific conditional knock out mice

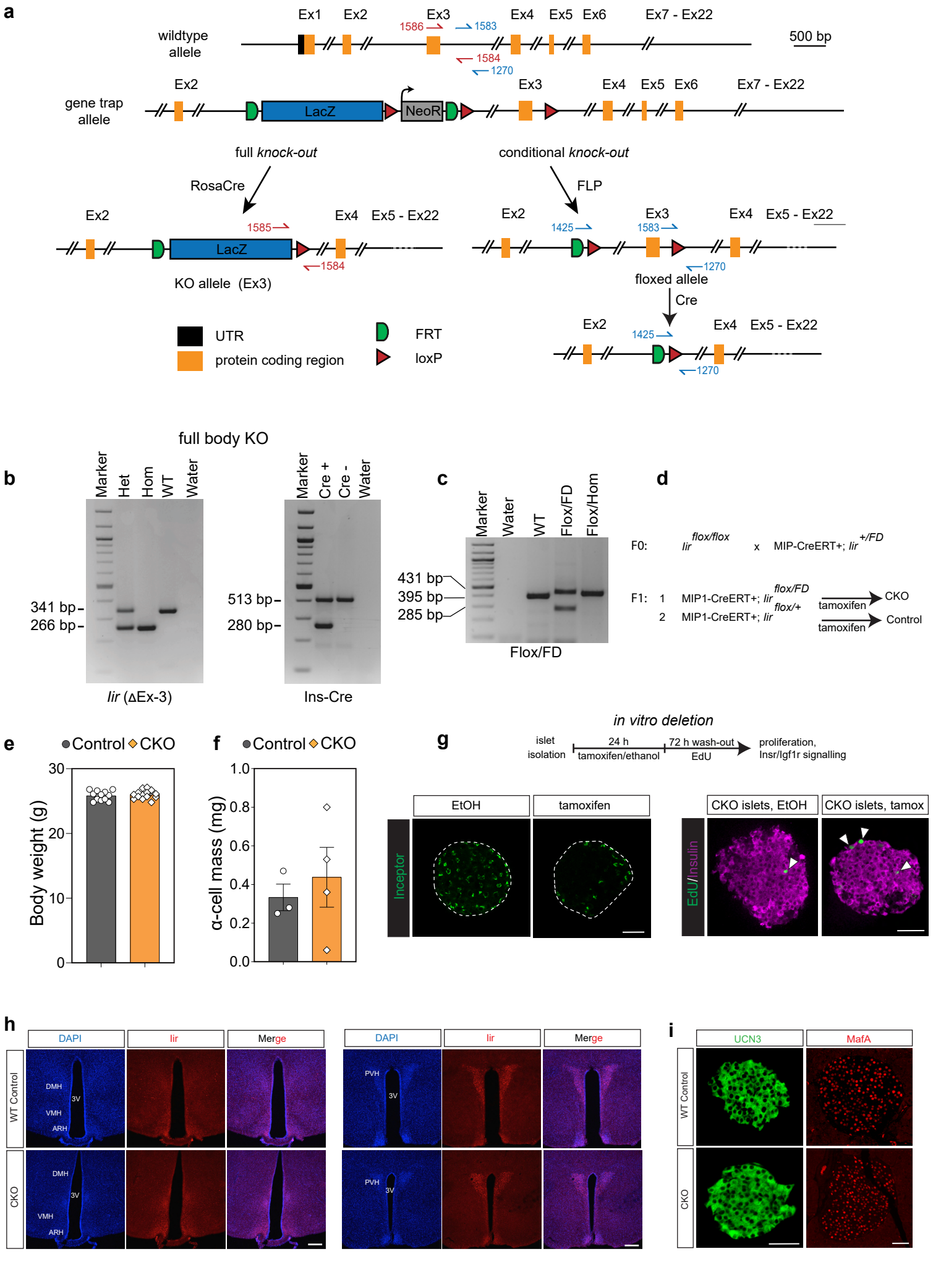

Extended Data Fig.6 | Inceptor routes in the secretory pathway and is quickly internalized to the Golgi-ER-lysosome compartment

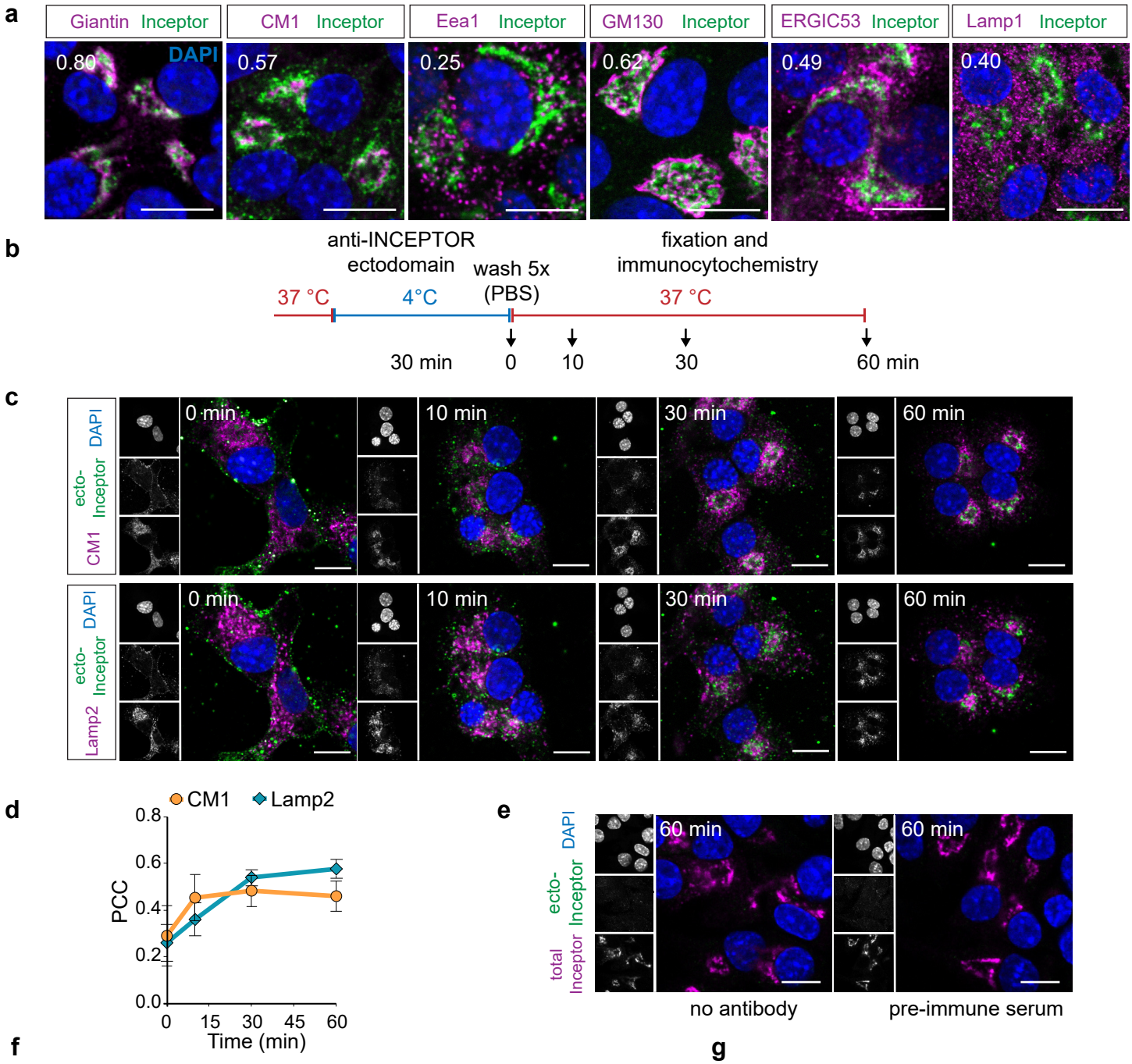

Extended Data Fig. 7 | Interaction of Inceptor with Insr /Igf1r and reduced uptake of labelled insulin in *lir*-Min6 knock out cells

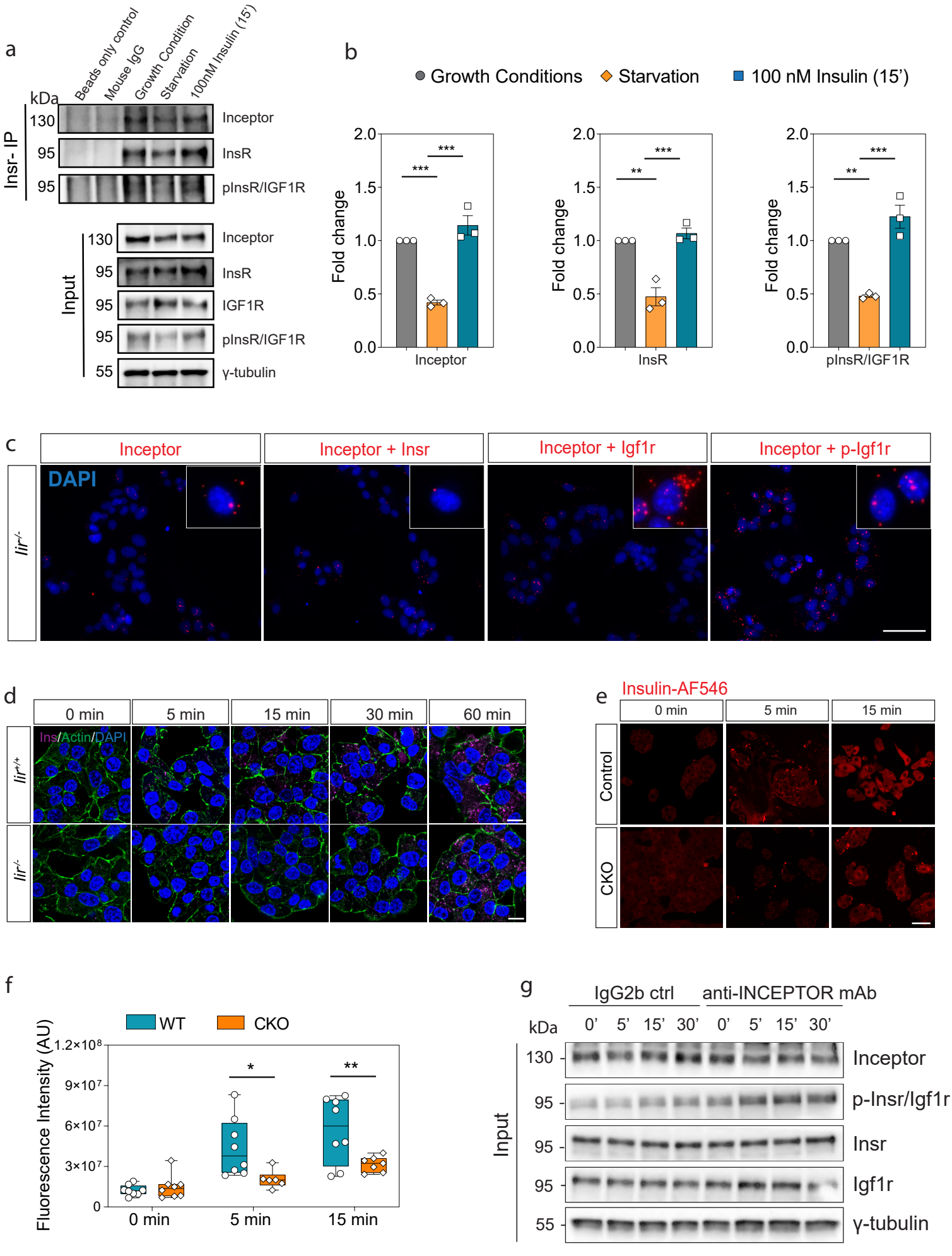

Extended Data Fig. 8 | Inceptor directly interacts with pAP2M1 and regulates AP2 mediated endocytosis of Insr/Igf1r

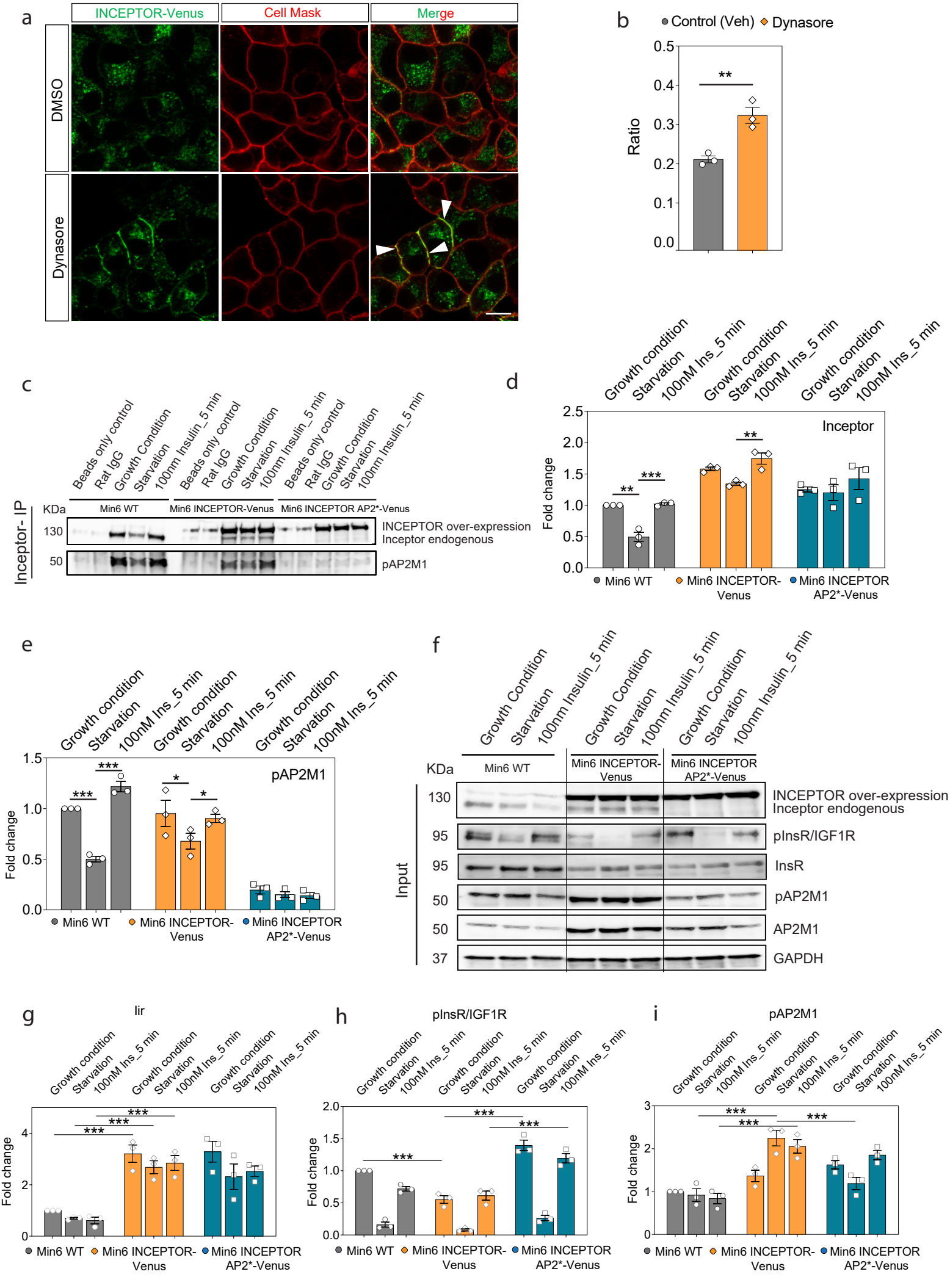

Extended Data Fig. 9 | Effect of INCEPTOR monoclonal antibody on human EndoC-βh1 cell line